Conventional Precursors and Activators

Luiz Miranda de Lima, Susan A. Bernal, Yuyan Huang, Alastair T. M. Marsh, Elijah D. Adesanya, Tero Luukkonen, Juho Yliniemi, Guang Ye, and John L. Provis

Abstract Among the various examples of sustainable construction materials explored in scientific literature, alkali-activated materials excel as one of the most mature and reliable solutions for large scale applications. It consists on the combination of an alkaline source in liquid or solid state, and a partially-to-fully amorphous solid precursor. The combination of these components leads to the obtainment of a hardened material which resembles Portland-cement based products. The performance and durability of these alternative binders is highly dependent on their components and production methods, and multiple laboratorial- and industrial-scale examples have shown their capability of outperforming conventional building materials. Practical challenges with variations in chemistry and mineralogy of raw materials, and the global utilization of prescriptive standards for structural building materials, hinder a wider utilization of these binders, and the efforts of the scientific and applied industry communities in overcoming these barriers is detailed throughout this report. This chapter provides an overview of alkali-activated binders, summarizing the main characteristics of their components, their reaction mechanisms, their challenges, and the expected advances of the technology with respect to one-part binders.

Keywords Fly ash · Blast furnace slag · Metakaolin · Dissolution kinetics · Microstructure · Dry-mixing · Co-milling

L. Miranda de Lima (✉) · G. Ye
Section Materials and Environment, Department of 3Md, Faculty of Civil Engineering and Geosciences, Delft University of Technology, Delft, The Netherlands
e-mail: luiz.miranda@paebbl.com

L. Miranda de Lima
Paebbl BV, Rotterdam, The Netherlands

S. A. Bernal · Y. Huang · A. T. M. Marsh
School of Civil Engineering, University of Leeds, Leeds, UK

E. D. Adesanya · T. Luukkonen · J. Yliniemi
Fibre and Particle Engineering, Faculty of Technology, University of Oulu, Oulu, Finland

J. L. Provis
Laboratory for Waste Management (LES), Paul Scherrer Institute (PSI), Villigen, Switzerland

G. Ye and F. Dehn (eds.), *Mechanical Properties of Alkali-Activated Materials*, RILEM State-of-the-Art Reports 46, https://doi.org/10.1007/978-3-032-07116-3_3

1 Introduction

Alkali-activated materials (AAMs) comprise binders formed by a chemical reaction process involving two components: a precursor and an activator [1]. The former is represented by silicates (usually aluminosilicates) of intermediate-to-low Ca content, either obtained as natural minerals or industrial byproducts, and often with a crystallographically disordered structure; and the latter is represented by alkaline sources, in either solid or liquid states [2, 3]. When these components are mixed in an aqueous media, a hardened cementitious matrix—similar in mechanical and binding properties to the hydrates formed during the hydration of Portland cement (PC)—is obtained, and the characteristics of the final binder are dependent on the nature of the initial raw materials used [1, 4, 5]. This reaction differs from those of PC hydration, as it requires the use of the added alkaline constituents to promote the *activation* of the precursor i.e. the dissolution of minerals via breakage of the amorphous structure—prior to the precipitation of reaction products.

The reaction potential of a precursor is dependent on the volume and chemical composition of the reactive fraction it contains—whether glassy or/vitreous or otherwise structurally disordered. Within the reactive fraction, the main expected components are SiO_2, Al_2O_3, and CaO, with minor quantities of MgO and Fe_2O_3 having an important role in the formation of secondary reaction products [6–8]. In some AAM formulations, particularly the "one-part or just-add-water" binding systems discussed in Sect. 4, soluble alkali metal compounds are included in solid form with (or in) the precursor. The reactivity of the precursor is important in the design of optimized mixtures, as the alkalinity level of the solution required to promote the reaction changes according to the reactivity of the precursors [9, 10]. Conventionally, precursors are classified as low-Ca and high-Ca materials. In general, the silicate structure of low-Ca materials is significantly polymerized, resulting either in partially-ordered layered silicate structures (e.g. in calcined clays) or in dense glass frameworks which require strong basic solutions to promote their breakage [11, 12]. High-Ca precursors tend toward a more disordered and depolymerized structure, as the presence of Ca destabilizes the continuous structure of SiO_2 and Al_2O_3 and promotes a less compact structure. Therefore, milder alkaline conditions are implemented to overcome energy barriers and promote the dissolution of these precursors [13–15].

The distinction of these two precursor classes is accompanied by differences in the mechanisms of reaction and in the type of phases precipitating upon the alkali-activating reactions. As shown in Fig. 1, under moderate alkaline conditions, Ca-rich materials promote the formation of calcium silicate hydrate (C–S–H) type gels (which are the main hydration product formed in PC-based reactions), and their variants. These gels can be modified in two ways: by the incorporation of Al, supplied by precursors which normally have higher Al_2O_3 contents than PC, resulting in the formation of calcium aluminosilicate hydrate (C–A–S–H) type gel; and by the uptake of alkaline elements resulting in the precipitation of sodium/potassium-bound calcium (alumino)silicate hydrate (C–N/K–A–S–H or C–N/K–S–H) gels—where N and K stand for Na_2O and K_2O, respectively [16–19]. The second group of precursors,

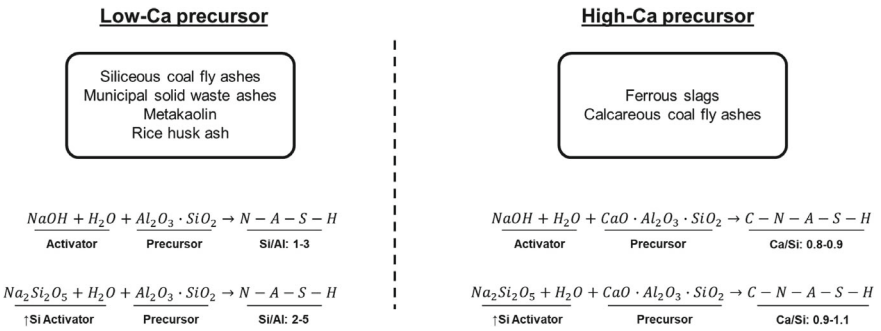

Fig. 1 Conceptual chemical reactions of alkali-activated materials, considering the Ca content of the precursor and activator—elemental ratios obtained from [6, 20–24]

comprised of Al- and Si-rich materials, results mainly in the formation of aluminosilicate hydrate (N/K–A–S–H) type gels [25–28], which is often aided by the implementation of more aggressive conditions—high alkalinity and/or curing temperatures above ambient. Additionally, secondary phases including layered double hydroxides or zeolites may also be formed depending on the exact composition of the precursors and activation conditions adapted [27].

This chapter will provide a summary of the main aspects of alkali-activated materials. The first section will cover the main raw materials utilized in such binders, explaining the differences in chemistry and mineralogy among precursors, and choice the importance of selecting the correct activator according to the each precursor. In sequence, a description of all phenomena involved in alkali-activating reactions will be given, covering all stages since early moments, with the dissolution of the precursors and initial precipitation of reaction products, until the development of mature microstructures, whilst evaluating the influence of different factors in the kinetics of reaction. Finally, the Chapter will provide a summary of the reaction mechanisms and most recent developments within the field of one-part alkali-activated materials, describing the advantages and challenges of these systems.

2 Conventional Raw Materials

2.1 Precursors

Considering chemistry and microstructure requirements, a vast list of materials present the potential to be used as precursors for alkali-activation, either alone or in combination with others in blended systems [29–36]. The majority of these materials are obtained as byproducts from primary industrial processes, thus reducing issues concerning extraction of non-renewable sources, high-energy demanding and high CO_2-emitting processes in their production chain. However, despite the cited

environmental advantages, the byproduct nature of these precursors poses extra challenges in the production of AAMs. Mostly, their mineralogy (particularly the fraction of reactive material) and chemical composition are dependent on the location of the raw material source and the primary industrial processes from which they are derived. It is also essential that the available volumes of materials are sufficient to make the design of an alkali-activation process economically worthwhile in the longer term. Some precursors will require extra beneficiation steps aiming to enhance their reactivity and/or remove deleterious constituents (either due to hazard to the end user, or because they interfere with the alkali-activation process), representing additional costs and extra embodied carbon emissions. While some have well established and mature beneficiation processes—e.g. coal fly ashes and blast furnace slags—new and unconventional precursors still require extra attention and research before optimized treatments are implemented. In this scenario, extensive research must be performed in order to design cost-, energy- and environmental-efficient beneficiation stages. However, the focus of this chapter is mainly on the description of the properties of conventional materials, so beneficiation routes will not be explored in detail.

The diagram in Fig. 2 details the typical compositions (considering CaO, SiO_2 and Al_2O_3 as the three main oxide components) of several materials that are commonly mentioned in literature as precursors, along with their primary production processes in the case of industrial byproducts. Among the available options, four materials show the most relevant commercial potential: coal fly ashes, blast furnace slags, metakaolin and silica fume, which are defined as conventional precursors and will be discussed in more details in this chapter. These precursors have been used for producing AAMs implemented in large-scale projects for over 60 years [1, 37, 38], and still represent a large portion of the current research efforts concerning optimization, performance enhancement, and improvement of service life of these binders. Other potential precursors, called non-conventional precursors, will be discussed in Chap. "Non-conventional Precursors and Activators".

Coal Fly Ashes

Coal fly ashes[1,2] are obtained by the combustion of pulverized coal in thermo-electrical power plants. Following specifications such as ASTM C618 [39] or EN 197-1 [40], fly ashes are divided in two classes according to their composition: calcareous, or class C fly ashes, which presents higher levels of CaO (above 10 or 18 wt.% depending on the standard used) with the remainder of the oxide analysis being mainly SiO_2, Al_2O_3 and Fe_2O_3; and siliceous, or class F ashes, with lower CaO content and more dominant silicate phases. The differences in chemistry arise mainly from the source of coal under combustion. The first group is usually obtained by the processing of sub-bituminous coal [41, 42], while the second group is often

[1] For the remainder of the chapter, the term "fly ash" will be used simply to describe coal fly ashes, without mentioning the natural extension to co-combustion ashes explicitly each time.

[2] Ashes from the co-combustion of coal with other materials, e.g. different biomass sources, are also included in standards of coal ash up to a certain blending degree—maximum allowed quantities differ between different standards.

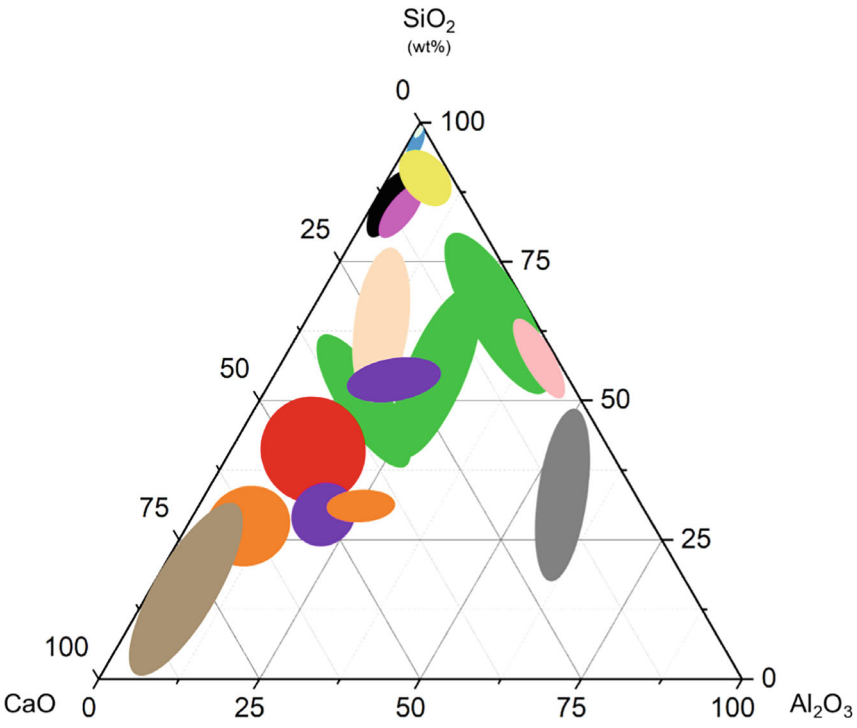

Primary industrial process	Resulting by-product – potential precursor
Production of steel and pig iron	Blast furnace slags
Thermal power plants	Coal fired fly ashes
Production of ceramic materials	Metakaolin
Biomass-derived ashes	Rice husk ashes
	Sugar cane bagasse ashes
	Palm oil fuel ashes

Primary industrial process	Resulting by-product – potential precursor
Production of aluminium	Red mud*
Production of Fe-Si alloys	Silica fume
Municipal wastes	Municipal solid waste incineration ashes
	Recycled glass
	Wood construction ashes
	Paper sludge ashes
	Sewage sludge ashes

Fig. 2 Distribution of chemical composition, considering CaO, SiO_2 and Al_2O_3, of the most cited precursors in AAM systems. Image from reference [45], Author's copyright. * Red mud presents significant amounts of Fe_2O_3 up to 50 wt.%

the result of the combustion of coals of higher grade—anthracite and bituminous coals [43, 44].

The schematic process of generation of fly ashes is illustrated in Fig. 3. In thermal powerplants, coal is initially ground and pulverized before being added into the boiler. The fine crushed coal is fed into the boiler which is blown with hot air, promoting the combustion of the feedstock and the obtainment of steam for generation of electric

Table 1 Distribution of oxides, atomic ratios and amorphous degree of fly ashes, slags and metakaolin reported in scientific literature

Precursor	CaO (wt%)	SiO2 (wt%)	Al2O3 (wt%)	Ca/Si	Amorphous content
Calcareous fly ash*	20-28	21-41	14-11	0.53-1.43	53-89%
Siliceous fly ash*	1-14	36-67	16-39	0.01-0.43	44-86%
Granulated blast furnace slag**	30-56	21-41	4-18	0.92-2.86	> 95%*
Metakaolin	-	52-56	44-48	-	-
Silica fume	< 1	> 96	< 0.5	< 0.01***	-

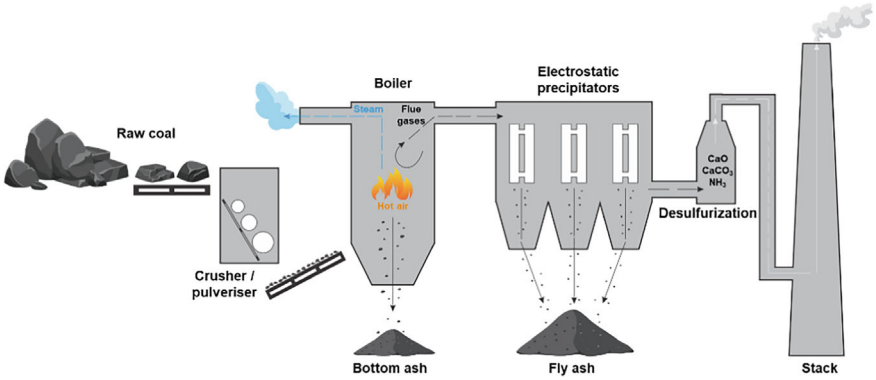

Fig. 3 Schematic production processes of primary sources of coal fly ash. Image from Ref. [45], Author's copyright

energy. After combustion, droplets of fused material are formed by the melting of the non-combustible inorganic compounds, and are exhausted from the boiler along with flue gases generated in the process. The solid portion of the unburnt material is captured and separated from the gases by electrostatic or mechanical separation, while a chemical process, aided by sorbent materials, promotes the flue gas desulfurization (FGD), which leads to the obtainment of valuable byproducts—e.g. synthetic gypsum and the release of less harmful gases to the stack. The fused material is forced to cool down rapidly, forming the typical spherical shape and vitreous nature of the fly ash particles [41]. Along with fly ashes, coal bottom ashes are also formed in the boiler as a secondary byproduct in the combustion process. Coarser pieces of unburnt residues, generally up to 20% of the total volume of combustion wastes, settle at the bottom of furnace. In general, these materials are less valuable for applications as cementitious binders, as they require additional grinding steps to enhance their reactivity. For that reason, bottom ashes are mostly used as fine aggregates rather than as part of the binder phase [46, 47].

Table 1: Distribution of oxides, atomic ratios and amorphous degree of fly ashes, slags and metakaolin reported in scientific literature. The schematic process of generation of fly ashes is illustrated in Fig. 3. In thermal powerplants, coal is initially ground and pulverized before being added into the boiler. The fine crushed coal is fed into the boiler which is blown with hot air, promoting the combustion of the feedstock and the obtainment of steam for generation of electric energy. After combustion, droplets of fused material are formed by the melting of the non-combustible inorganic compounds, and are exhausted from the boiler along with flue gases generated in the process. The solid portion of the unburnt material is captured and separated from the gases by electrostatic or mechanical separation, while a chemical process, aided by sorbent materials, promotes the flue gas desulfurization (FGD), which leads to the obtainment of valuable byproducts—e.g. synthetic gypsum and the release of less harmful gases to the stack. The fused material is forced to cool down rapidly, forming the typical spherical shape and vitreous nature of the fly ash particles [41].

Along with fly ashes, coal bottom ashes are also formed in the boiler as a secondary byproduct in the combustion process. Coarser pieces of unburnt residues, generally up to 20% of the total volume of combustion wastes, settle at the bottom of furnace. In general, these materials are less valuable for applications as cementitious binders, as they require additional grinding steps to enhance their reactivity. For that reason, bottom ashes are mostly used as fine aggregates rather than as part of the binder phase [46, 47].

The fraction of amorphous material in fly ashes—which is generally identified as the main reactive fraction in these materials—varies from 40 to 90% of the total volume. These differences arise from different characteristics of the initial source material and the combustion process, such as coal grade, particle size distribution, and cooling conditions of the molten material. Within a single batch, it is possible to identify differences among the collected particles, as particles of different sizes display different quenching rates according to their surface area. More rapid cooling is obtained for smaller particles, increasing their final amorphous fraction, while slower cooling rates in coarser particles might result in internal recrystallization of the inner material, favouring larger residual crystalline regions [48, 49]. Mostly, quartz is the main remaining mineral phase found in fly ashes, since SiO_2 is either the first or second main inorganic component in coals. Minor quantities of mullite, hematite, calcium aluminates, and lime can also be [50–52]; the latter two are mainly observed in Ca-rich ashes and are also part of the reactive fraction of the ash.

The co-combustion of coal with other materials is a trending practice in power-plants. While it lowers the CO_2 emissions attributed to energy generation, it also leads to some changes in the compositions of the molten material that becomes the ash; this may be either beneficial or detrimental. For instance, Sarabèr [50] and Wu et al. [51] demonstrated that the use of agricultural wastes, such as poultry dung, and of rejects from paper production, can increase the CaO content of the ashes, but the glass quantity is reduced by approximately 25%. Similarly, Faleschini et al. [52] reported an increased content of unburned material when refuse-derived fuels (RDF)—mainly papers and plastics—are burnt in combination with coal, which results in delayed setting and decreased strength of concrete when used as SCM.

Due to the large number of variables in their primary production process, fly ashes present the largest variation in chemistry and amorphous fraction among the other conventional precursors, as shown in Table 1—see Table 25.3 in [53] for details compositional limits of SCMs and precursors in alkali-activated systems. While the composition of siliceous fly ashes is dominated by SiO_2 and Al_2O_3, calcareous fly ashes represent an intermediate material in terms of chemistry. The higher contents of CaO promote changes in the structure of the amorphous regions, and this class of ashes is considered as an intermediate between blast furnace slags and siliceous fly ashes with respect to their reaction potential.

Blast furnace slag

Blast furnace slags are obtained as valuable byproducts during the production of pig iron, which is the first component in the manufacturing chain of steel [1]. Pig iron is formed by the thermo-chemical reduction of iron ores in furnaces constantly blasted

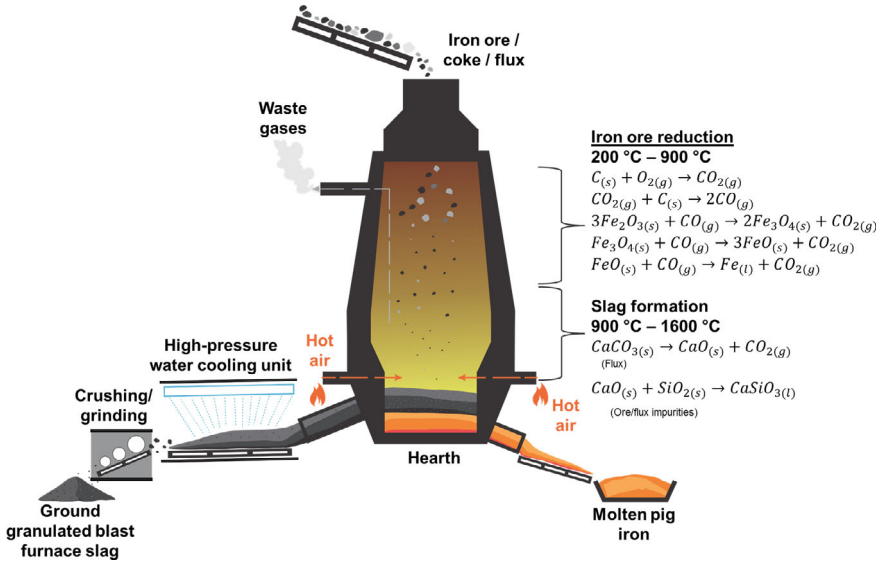

Fig. 4 Schematic production processes of primary sources of blast furnace slag. Image from Ref. [45], Author's copyright

with hot air, as illustrated in Fig. 4. The mineral ore and the coke are added at the top of the furnace and becomes exposed to different temperatures before reaching the bottom. The first step of the reaction is the formation of carbon monoxide by sequential reactions of coke with oxygen, which leads to the reduction of Fe_2O_3–FeO at temperatures below 1000 °C shortly after the material is supplied. The mineral passes through a thermal equilibrium stage in the middle of the furnace, and the complete reduction occurs at the bottom at 1500 °C, with the separation of metallic Fe from contaminants. Along with iron ore, the furnace is supplied with flux material [54]. The melting stage is aided by the fluxes—limestone and dolomite—as they induce a reduction in the viscosity of the molten material. Alongside the metallic Fe, the contaminants of the ore react with coke, fluxes, and the hot air inside the furnace to form an oxide phase called *slag*, usually rich in calcium silicate phases, and both liquid slag and pig iron set in the bottom of the furnace in a region called hearth. The two components are then physically separated from the molten iron in a skimmer [27, 55], and individual outlets separate them.

At the end of the melting process, the temperature of the slag is approximately 1600 °C, and the cooling method is essential to determine its properties and reactivity. Conventionally, high-pressure water-cooled granulation is used to enhance the heat exchange and the cooling rate, promoting a larger volume of amorphous material at the end of the process. Historically, some slags also used to be slow-cooled, but this is rarely done now because of the loss of the cementitious value of the slag as it crystallizes during slow cooling. Air-cooling and pelletization processes are also gaining popularity, and can produce a broadly comparable material. Finally, the

cooled slag is ground into a fine powder before being suitable to be used as a binder in cementitious systems—due to the overall beneficiation process, it is also commonly termed as ground granulated blast furnace slag (GGBFS).

Slags commonly have CaO as their main component, followed by SiO_2, Al_2O_3 and variable quantities of MgO. They also contain a minor but important content of reduced sulfur, which has a strong influence on the redox chemistry of alkali-activated binders produced from slags. Although they are not as diverse as fly ashes, variations in chemistry can still be expected in slags due to the source of the iron ore, the composition of the fluxes and the use of burning gases to enhance the capacity of the blast furnace [56, 57]—see Table 1.

The combination of higher CaO and amorphous contents, compared to fly ashes and other precursors, leads to the classification of this precursor as the closest one to cementitious (latent hydraulic) in nature. The reactivity of slags is usually a function of its *basicity index*, which is expressed by the CaO/SiO_2 or $(CaO + MgO)/SiO_2$ ratios of the precursor [58–61], as this definition is dependent on the approaches chosen by different authors. In essence, the basicity of a slag distinguishes precursors as either basic or acid [59], with the former presenting higher reaction potential. The presence of significant amounts of CaO and low contents of SiO_2 promotes the formation of similar phases to the ones present in clinker [58], thus facilitating the reactions with alkaline solutions and making this a valuable raw material for both AAMs and blended cements. It is important to state that, while a high basicity index increases reactivity, it also promotes a higher viscosity of the molten slag [62, 63] and creates challenges during its production.

Metakaolin

Metakaolin is a metastable mineral phase produced by the thermal treatment (calcination) of kaolinitic clays. These clays can be obtained directly by the extraction of natural deposits or by the reutilization of wastes from mining, or from the manufacturing of paper, ceramics, and refractories. Kaolinite is comprised of continuous sheet-like structures of SiO_2 and Al_2O_3. In one layer, Al is found in octahedral coordination with repeating AlO_6 basic units that carry bound hydroxyl groups, while the second layer is composed of SiO_4 tetrahedra arranged in continuous sheets of six-membered rings [64, 65]. As shown in the sketch of Fig. 5, Al is partially bound to the SiO_2 structure of the adjacent layer and to H in the opposite face forming $AlO_2(OH)_4$ sheets, and these continuous structures are stacked with a distance of approximately 7.2 Å between two sheets [66].

The calcination of kaolinite enhances its pozzolanic reactivity, making it a suitable precursor for alkali-activation [46]. The thermal treatment promotes the dehydroxylation of the original framework and reduces the ordering of the continuous Al_2O_3–SiO_2 sheets, although the layered structure is retained so the material is not truly "amorphous" [67]. The resulting material is a disordered aluminosilicate mineral [68, 69], and the reactive portion is slightly different than slags and fly ashes due to the nearly negligible amounts of network modifying oxides in the original clay—see Sect. 3.1 for more details.

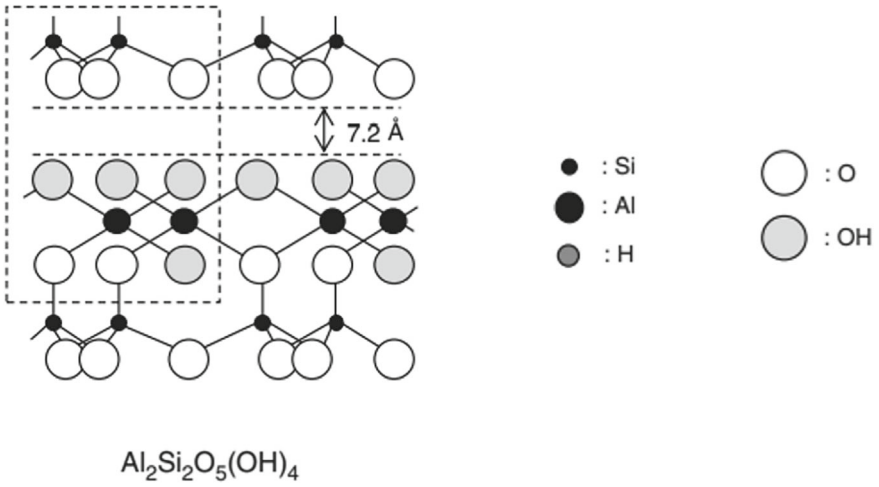

Fig. 5 Schematic illustration of the structure of kaolinite. Adapted from [66], copyright Elsevier

The features of the reactive portions are dependent on the temperature and duration of the calcination. In general, higher temperatures promote a more significant breakdown of the original structure. The main structural changes are observed in the Al_2O_3 layers, which convert the octahedral coordination into the less stable AlO_4 and intermediate AlO_5 units [70, 71]. The loss of chemically bound water and destabilization of the original structure begins at approximately 550 °C, as determined by White et al. [72] via inelastic neutron scattering, and occurs up to 800 °C [73–75]. A significant change in the Al coordination starts at approximately 600 °C [66], with a continuous increase of four- and fivefold coordinated Al at the expense of AlO_6, up to approximately 900 °C [70]. Above this threshold value, the formation of sixfold coordinated units is again observed, and the more stable mineral phase mullite is formed [76].

Structural changes are also observed outside this temperature window, depending on the heating rate and length of the thermal treatment. As observed in the plot in Fig. 6, the dehydroxylation of kaolinite achieves similar weight loss, after 6 h of treatment at 500 °C, to values measured with continuous heating up to 700 °C, as measured per thermogravimetric analysis. Similarly, Khaled et al. [77] reported that a similar reactivity was achieved for clays treated for 1 h at 500 °C compared to a 30 min-step at 600 °C. On the other end of the process, Sanz et al. [71] determined that a long treatment of 36 h, at 850 °C, was sufficient to replicate quantity of mullite formed after a 3 h treatment at 980 °C.

The final chemical composition of metakaolin is fully dependent on the purity of the original clay. In natural deposits, kaolin is usually found to be combined with quartz, as well as some feldspars, iron-containing minerals, and other clays, which can impact the final reactivity of the treated metakaolin [46, 66, 71]. In industrial processes, the sourced mineral often goes through various beneficiation treatments, as

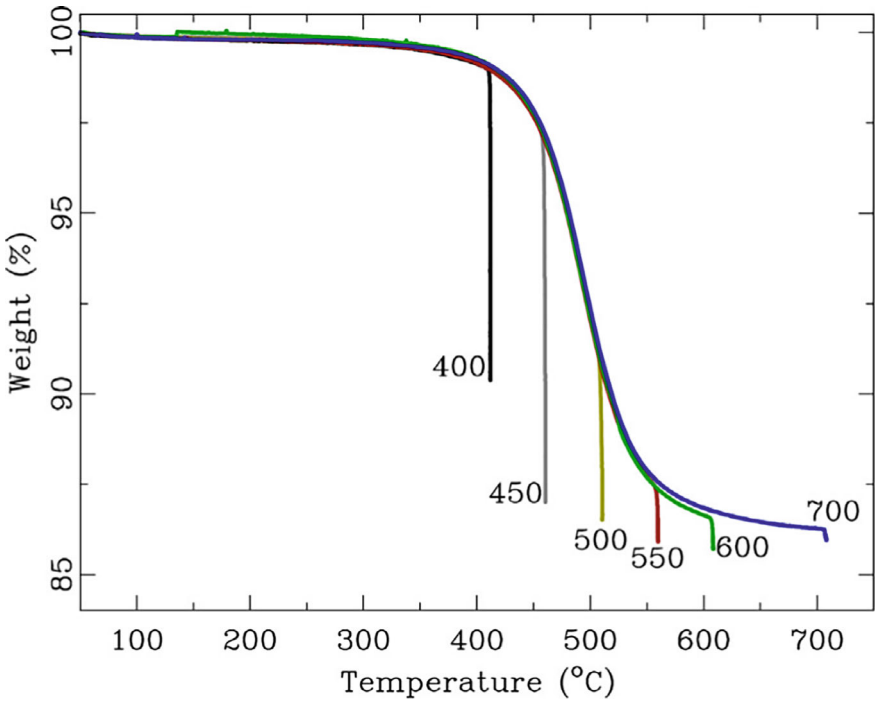

Fig. 6 Thermally induced weight loss of pure kaolinite, measured by thermogravimetry, with a heating rate of 5 °C/min followed by an isothermal hold for 6 h at the indicated temperatures. Adapted from [72], copyright Elsevier

a mineral of high purity is usually required [78, 79]. However, this high purity is relatively less important when considering utilization as an alkali-activation precursor, which means that impure kaolinitic clays can also become valuable. In general, the composition of metakaolin does not present variations as wide as fly ashes, as detailed in Table 1.

Silica fume

Silica fume is obtained as a valuable byproduct from the production of elemental silicon and ferrosilicon alloys. The same production principle is used in the two processes, but the different raw materials implemented in each promote differences in the final characteristics of the byproduct. In both conditions, high-purity quartz is reduced under high temperatures (approximately 2000 °C) in electric arc furnaces, generating silicon dioxide vapor, which is then precipitated by cooling into nanoscopic particles [61]. Silica fume typically contains more than 85–95% SiO_2, with an average particle size of about 0.1–0.5 μm. It is a very reactive, rather pure source of silica that is widely used in blends with Portland cement as the high-reactivity pozzolan commonly available; in alkali-activation it is generally used as a supplementary silica source to adjust mix compositions, rather than as a primary

precursor in its own right, because the absence of aluminium means that it does not form an effective N–A–S–H type gel [80].

2.2 Selection of Activators

Out of the several reported activators used in alkali-activated binders, alkali hydroxides, silicates and carbonates are the most explored due to their high reactivity and relatively low cost [1, 81]. Activators play the joint role of catalyst and reaction participant, facilitating the initial dissolution process of precursors and accelerating the steady formation of hardened binders [82]. These components of the mix must provide sufficient alkalinity to promote the breakage of the glass network of the precursors, and be optimized to maintain appropriate fluidity to favour the growth of stable reaction products [83]. In the majority of applications, activators are prepared in a separate step prior to mixing with precursors, promoting a homogeneous distribution of reactive alkaline species within a liquid media. Commercially available activators are already supplied in liquid form by manufacturers, facilitating the preparation of AAM-mixtures. Extensive research has also been dedicated to the implementation of one-part geopolymers by utilization of solid activators mixed with particles of the precursor material [81–83]; see Sect. 4 for more details of that type of process, while the remainder of this section is dedicated to two-part (liquid activator) systems.

The efficiency of an activator requires the correct choice and dosage of the reactant material, factors which are directly correlated with the characteristics of the precursor. For instance, Ca-rich materials display different dissolution behavior compared to precursors mainly based on aluminosilicates [84, 85], as the higher degree of depolymerization of the glass network requires lower alkalinity levels to promote dissolution. In general, increased concentration of alkalis in aqueous media promotes a stronger cohesion of the hardened matrix and consequently improves the mechanical properties of AAMs [2]. However, this enhanced performance is expected only up to a threshold value, and the excess of alkaline ions can lead to additional issues in terms of evolution of microstructure, service-life and lifecycle assessment [9, 86, 87]. An extremely high pH of the activator can induce flash setting and increase the viscosity of the activating solution [27], which hinders a continuous dissolution of the precursor and results in a coarse microstructure, compromising the final performance; the excess of alkaline ions can more easily trigger the formation of expansive products via alkali-silica reactions or the occurrence of efflorescence [2, 3], which further shortens service life of concrete elements. Finally, excess of activators can decrease the environmental profile of the binder, as activators present the highest global warming potential among components of AAM mixtures [88].

The majority of activators used in a practical sense are sodium based, either in the form of hydroxides, carbonates, or silicates. While in the first two cases one always refers to the molarity of the alkaline solution and ratios of Na_2O to the precursor (n, or mass of alkaline oxide per 100 g of precursor), the latter case is also strongly influenced by the silica modulus (M_s) of the solution, calculated by Eq. (1):

$$M_s = \frac{[SiO_2]}{[Na_2O]} \quad (1)$$

When sodium silicate (also termed waterglass) solutions are used, mixing procedure and performance are directly influenced by the Ms of the activator. When used in excess, a critical issue appears with the rapid workability loss of alkali-activated slag mixtures [84]. Limited setting time and uncontrolled stiffening process have been frequently reported in silicate-activated slag [89–91], leading to great challenges in the mixing, delivery, pumping, casting, and consolidation of some fresh mixtures. Previous studies have illustrated the significant influence of silicate modulus (Ms) on the mineralogical and chemical properties of reaction products in alkali-activated slag [92, 93]. It has been suggested that the rapid setting is attributed to the precipitation of primary C–(A)–S–H type gels [94–96].

It should also be noted that numerous research studies use the shorthand "Na_2SiO_3" as an abbreviation for sodium silicate in describing mix designs. In most cases this is done incorrectly, as liquid sodium silicates are not commercially supplied at this 1:1 molar ratio of SiO_2:Na_2O (although some solid sodium metasilicates are), due to the tendency of sodium silicate liquids at this concentration to precipitate [97]. Common liquid silicate compositions include molar ratios M_s of 2.0 or 3.3, although other ratios are also available. This imprecision in description by many researchers causes difficulty in interpretation and reproducibility of the technical literature, as the chemical notation is used incorrectly in so many cases, and it is strongly recommended that this be treated with more care in future studies.

Potassium-based activators are also used, and perform largely equivalently to their sodium counterparts, although with some differences in the relative rates of dissolution and reprecipitation aspects of the reaction process, and also some alteration in viscosity of the paste. Potassium silicate and hydroxide are more expensive than sodium silicate and hydroxide, which means that they are mainly considered for use in higher-value, lower-volume applications including "ceramic-type" applications or nuclear waste immobilization.

3 Reaction Mechanisms and Influencing Factors

The wide range of solid precursors and processing parameters, discussed in the previous sections, introduces additional complexity to AAMs, as these conditions have crucial effects in the properties of fresh and hardened binders. While this brings a certain versatility to the technology, allowing fit-for-purpose formulations, each mix design differs from the others in terms of reaction mechanisms, hindering the applicability and marketability of the technology.

The reactivity of alkali-activated systems, as well as the evolution and final features of the microstructure, is largely dependent on the mixture design and on processing conditions. In a simplified way, the reactivity of precursors can be directly linked to the initial content of CaO, especially in the initial stages [1, 98]. High-Ca precursor

materials react more rapidly in environments with low or moderate alkalinity, such as when a carbonate or sulfate (near-neutral) activator is used [99, 100]. For comparison, when slag is utilized as an SCM in blended PC-based systems, faster reactions and strength development are usually observed in comparison to the implementation of metakaolin or fly ash [101–104]. This occurs because slags behave as *latent hydraulic* materials, i.e. in long periods they are expected to react in aqueous media containing only water. On the other hand, fly ashes and other low-Ca materials behave as *pozzolanic* materials due to their polymerized Al–Si-dominated structure, and require activating enhancing agents in AAM-systems—e.g. high alkalinity, and sometimes also benefit from higher reaction/curing temperature [12, 105]. These distinct mechanisms, arising from differences in the amorphous framework, have direct impacts on reactivity and final reaction products, which will be discussed in the next sections.

3.1 Structure of Disordered Portion of Precursors

The reaction potential of a crystallographically disordered precursor in alkali-activation is often linked to the total volume and connectivity, and to the chemical composition of the amorphous portion [81, 106]. Additionally to the lack of long-range order, the atomic short-range organization of glass structures can be modified by the presence of several elements, and these alterations have a significant impact on the overall reaction process. A glass structure is basically composed of network forming (NWF) and network modifying (NWM) oxides, which differ in coordination and in roles within the framework [107, 108]. NWFs present stronger M–O bonds and are more thermodynamically stable, forming cohesive structures [107], where M stands for metallic elements.

In aluminosilicate glasses, which represent the reactive portion of blast furnace slag and fly ash, SiO_2 is the main NWF. Si presents a tetrahedral coordination (with SiO_4 as the basic unit), and each oxide of the network can be shared with other tetrahedra, forming different structural units [107]. Al_2O_3 partially displays the same behavior as SiO_2, as it can act as an NWF in fourfold coordination, and as a NWM in both fivefold and sixfold coordination [109, 110]. When acting as a network forming agent, Al substitutes one Si atom in tetrahedral structures forming $[AlO_4]^-$ sites, requiring the presence of charge-balancing (e.g. alkaline or alkaline-earth) cations to maintain the local electrical neutrality [107]. These Al–Si network-forming units are classified using the notation type $Q^n(mAl)$, with $0 \leq m \leq n \leq 4$—where n is number of connected SiO_4 units and m represents the amount of Al-substituted sites and can be identified using solid state ^{29}Si magic-angle spinning nuclear magnetic resonance (^{29}Si MAS NMR) [111]. As shown in Fig. 7a, b, each unit presents typical resonances ranging from approximately -50 ^{29}Si/ppm (with $n = 0$, in fully depolymerized sites) to approximately -120 ^{29}Si/ppm (with $n = 4$, in fully polymerized sites) [111, 112]. Additionally, ^{27}Al MAS NMR can be used to identify the three different Al–O units,

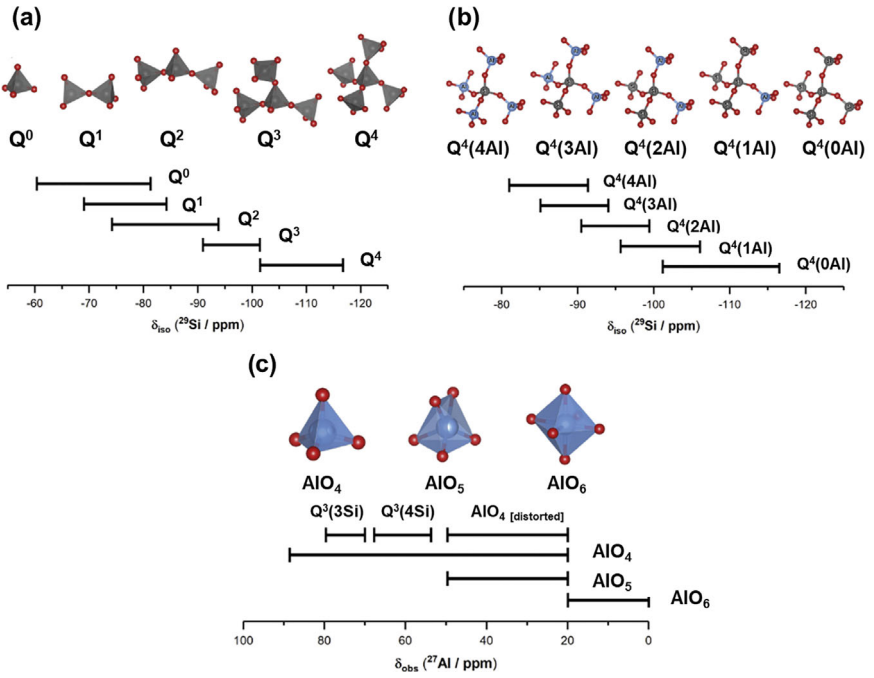

Fig. 7 Schematic illustration of structural units and their typical reflections in ^{29}Si and ^{27}Al MAS NMR experiments: **a** pure SiO_4 and **b** and Al-substituted SiO_4 units; **c** Al–O units. Adapted from [111], copyright Elsevier

as fourfold (Al^{IV}), fivefold (Al^{V}) and sixfold (Al^{IV}) coordination also have their own characteristic chemical shifts [111, 112] see Fig. 7c.

The core of the amorphous structure of a precursor is formed by a repetition of basic units of NWF oxides. Shared oxygen sites in between two tetrahedra are named bridging sites, and the connections made by these elements in the silicate network can be disrupted by the presence of NWM oxides of alkaline and alkaline-earth elements. These compounds promote the breakage of Si–O bonds in bridging points and form separate Si–O–M^+ bonds, following the reaction displayed in Eq. (2) [107]. The result is an even shorter range of atomic order by formation of non-bridging oxygen (NBO) sites in AAM-precursors, CaO, MgO, Na_2O and K_2O are the most common NWMs [107]. By reducing the total amount of bridging oxygens, NWMs decrease the overall cohesion of the microstructure and reduce the energy barrier required to initiate dissolution and further stages of reaction [113, 114].

$$\equiv \mathrm{Si} - \mathrm{O} - \mathrm{Si} \equiv + \mathrm{M_2O} \rightarrow \equiv \mathrm{Si} - \mathrm{O} - \mathrm{M}^+ + \mathrm{M}^+ - \mathrm{O} - \mathrm{Si} \equiv \qquad (2)$$

The depolymerization effect of NWM oxides has been described by many authors, and they induce a clear distinction between high- and low-Ca precursors, for instance. Fly ashes can present up to 90% Si Q^4 species and nearly no remaining individual

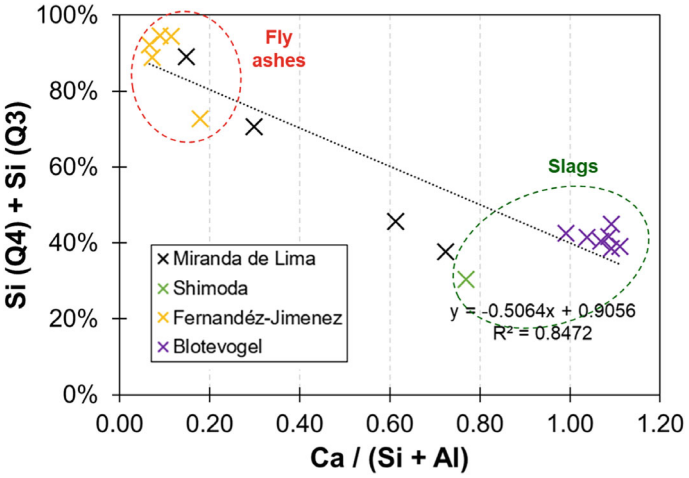

Fig. 8 Linear relationship between the content of Ca (molar basis in the precursor) and the quantitative distribution of Si Q^n sites in different precursors conventionally used in AAMs—data adapted from [99, 115, 116]. Image from Ref. [45], Author's copyright

SiO_4 (Q^0) units, while slags mainly display networks with short chain lengths (Q^1 and Q^2) [99, 115, 116]. As reported by Miranda de Lima [45], a quantitative determination of silicate units can be directly correlated with the fraction of Ca in precursors of different sources. The authors characterized the structure of glasses in the CaO–Al_2O_3–SiO_2 (CAS) system, comparing their findings with additional results reported in literature. Figure 8 shows the linear correlation established in that work, which successfully correlates the content of the most polymerized units ($Q^3 + Q^4$) with the Ca/(Si + Al) ratio of synthetic and commercial slags and fly ashes.

In addition to promoting the depolymerization of amorphous portions, Ca changes the main structure of the glass phases. The maximum 2θ angle value of the diffuse scattering, in X-ray diffraction (XRD) patterns, has been observed to display a direct relationship with the CaO content of the precursor. This correlation was first studied by Diamond [117], who reported a linear trend valid for low- and high-Ca fly ashes containing from 0.9 wt.% to 20 wt.% of CaO. McCarthy et al. [118] supported this correlation by creating a database of 178 samples from different sources in USA, which resulted in a similar, although not equally, strict trend—see Fig. 9a. In both cases, the linear relationship is interrupted at an upper CaO wt.% threshold of approximately 20 wt.%, as all calcareous ashes displayed similar maximum 2θ diffraction angles between 30 and 32°. A similar correlation with synthetic glasses mimicking the composition of slags was established by Goto et al. [119]. Those authors reported a linear relationship of the maxima diffraction intensity with CaO contents above 30 wt.%, which follows a similar slope as the majority of the fly ashes reported by Diamond, as shown in Fig. 9b.

The relationships described by the authors indicate the existence of two separate regions in both ends of Ca contents. Siliceous fly ashes display diffraction maxima

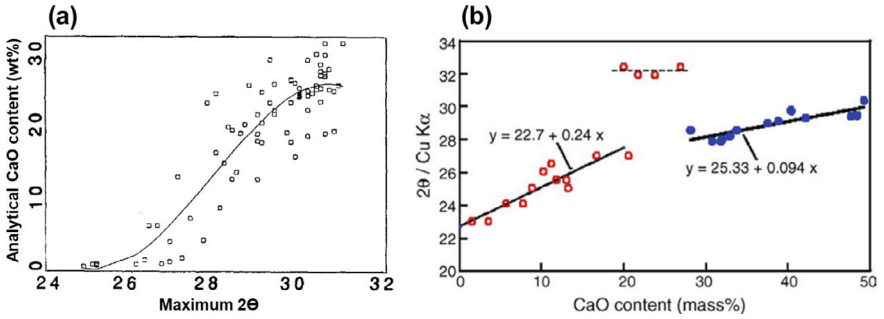

Fig. 9 Correlation of the maximum 2θ position with chemistry of synthetic glasses: **a** data adapted from McCarthy et al. [118] and **b**additional data adapted from Goto et al. [119] (copyright The Journal of the European Ceramic Society). Copyright The American Ceramic Society

close to aluminosilicate dominated structures, such as mullite (2θ = 25.97°; powder diffraction file (PDF)# 00-015-0776) and sillimanite (2θ = 26.19; PDF# 00-001-0626), and to pure SiO_2 phases like cristobalite (2θ = 21.95°; PDF# 00-011-0695). Similarly, the negligible Ca content in metakaolin pushes the maximum intensity of the diffuse scattering to values below 25° 2q, as reported by different source materials in different scientific publications [66, 69, 120–123]. Slags diffraction patterns often present reflections comparable to those observed in Ca–Al-rich phases such as gehlenite (2θ = 31.36°; PDF# 00-020-0199) and åkermanite (2θ = 31.13°; PDF # 00-035-0592), while calcareous fly ashes are in the intermediate region between both areas. As conventional precursors display variable levels of residual crystalline phases, it is easily assumed that the vitreous portion is composed of regions which did not convert into organized atomic arrangements due to high cooling rates. Consequently, the residual glass resembles what would be stable crystalline structures formed by the locally available atoms [124]. This observation is in agreement with several results available in the literature [11, 125–128], with mullite representing up to 22% [48] of the mineralogical composition of fly ashes, and slag displaying well defined residual presence of gehlenite, åkermanite and even tricalcium aluminate (C_3A) [129, 130].

3.2 Kinetics of Dissolution

In alkali-activated systems, the first stage of the reaction is the dissolution of the precursor, which starts immediately after contact with the alkaline activator [81]. Dissolution is a continuous process that promotes the breakage of covalent and ionic bonds from the glass network, releasing reactive aqueous species to the surrounding media. The reaction is prompted by the ionic strength of the liquid activating solution [3, 131, 132], and the rate of release of elements from the original framework is

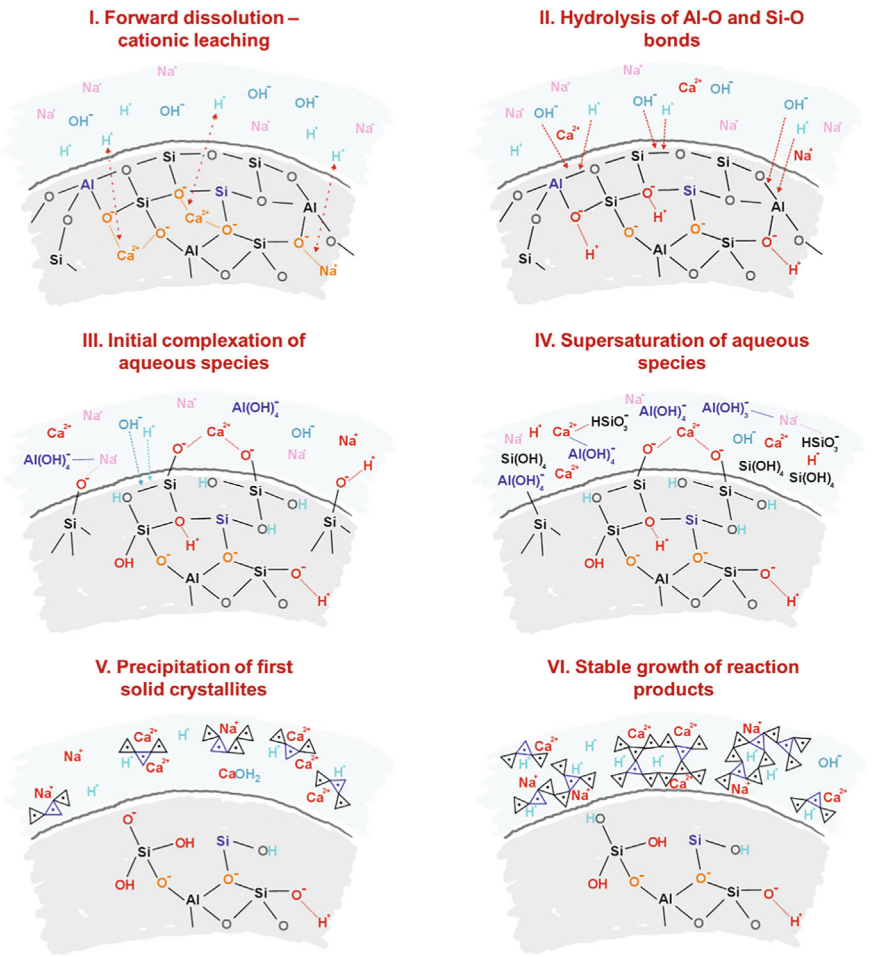

Fig. 10 Schematic illustration of the sequence of dissolution of precursors in alkaline solutions. Image from Ref. [45], Author's copyright

dependent on both the solution alkalinity and the polymerization degree of the glass network of the precursor [107, 110].

The scheme shown in Fig. 10 illustrates all the steps involved in the dissolution of precursors, covering the stage termed *forward dissolution period* prior to the stable precipitation of reaction products. Initially, the framework goes through a proton exchange mechanism (I.) between aqueous species and cations loosely bound to the glass network [81] identified with orange color. This triggers a significant release of Na^+ and Ca^{2+} to the aqueous media (II.)—identified with red color and is described as a cationic leaching process. Then, hydrolysis of primary and stronger covalent bonds of bridging oxygen atoms begins (II.), disrupting aluminosilicate chains or opening rings into smaller chains [133]. The intensity of this stage is directly linked

to the alkalinity of the aqueous media, credited to the concentration of OH^- species arising in environments with increasing pH. At this stage, the release of Al-species usually occurs earlier than release of Si-species, since Al–O bonds are weaker than Si–O bonds [131, 132]. The just-released cationic species are prone to interact with other aqueous species, forming complexes (III.), and with the course of time, the concentration of such complexes increases until nucleation of reaction products is observed (IV.) [81, 134]. The complexed ions combine among themselves and with other reactive species in the surrounding media to form the first nanosized units of solid products (V.) [135, 136], which will eventually coalesce and grow into stable solid products (VI.).

The influence of chemical composition on the initial stages of alkali-activating reactions is rather complex to determine quantitatively, since it involves the (very difficult) accurate replication of the scenarios occurring in very early stages of reaction. Such studies are performed in *far-from-equilibrium* conditions by using high solution to precursor ratios and focus mainly on the forward period prior to the precipitation of any reaction product. High-Ca compounds are expected to display higher dissolution rates [13–15], and therefore an enhanced reactivity. The initial cationic-exchange step makes Ca immediately available to be combined with others and form the first nuclei of reaction products [81]. Snellings et al. [137] and Schöler et al. [110] investigated the dissolution kinetics of synthetic glasses resembling blast furnace slag, siliceous and calcareous fly ashes in NaOH and KOH solutions, respectively. As shown in Fig. 11a, b, the authors reported forward dissolution rates of Si ($r_{+,Si}$) and Al ($r_{+,Al}$) up to 1.5 orders of magnitude higher for percalcic glasses when compared to low-Ca materials, establishing linear correlations between the dissolution of Si and Al with the fraction of Ca and the NBO/T of the original framework.

Zuo [138] also investigated the effect of the molarity of NaOH in the initial reaction kinetics of slag, and proposed the linear correlation shown in Fig. 11c, which establishes a relationship of the dissolution rate of Ca with the pH of the solution. The type of NWM oxide has been found to have little influence over the initial reactivity of AAMs. Hamdan et al. [139] compared the dissolution behavior of synthetic slags obtained in the $MgO–CaO–SiO_2–Al_2O_3$ system. With fixed Si and Al contents, those authors did not observe significant changes in dissolution rates arising from a gradual substitution of CaO by MgO, in agreement with the lack of changes in glass structure. However, the authors reported major changes in the subsequent stages of reaction, as an excess of MgO hindered the precipitation of silicate reaction products.

3.3 Pore Solution and Precipitation of Reaction Products

In the early stages of the alkali-activation reaction, after the precursors have dissolved to a sufficient extent to reach supersaturation and enable the formation of new solid products to start, the precipitation rate of reaction products is related to the dissolved concentrations and thus the dissolution rates of the main components of the precursor.

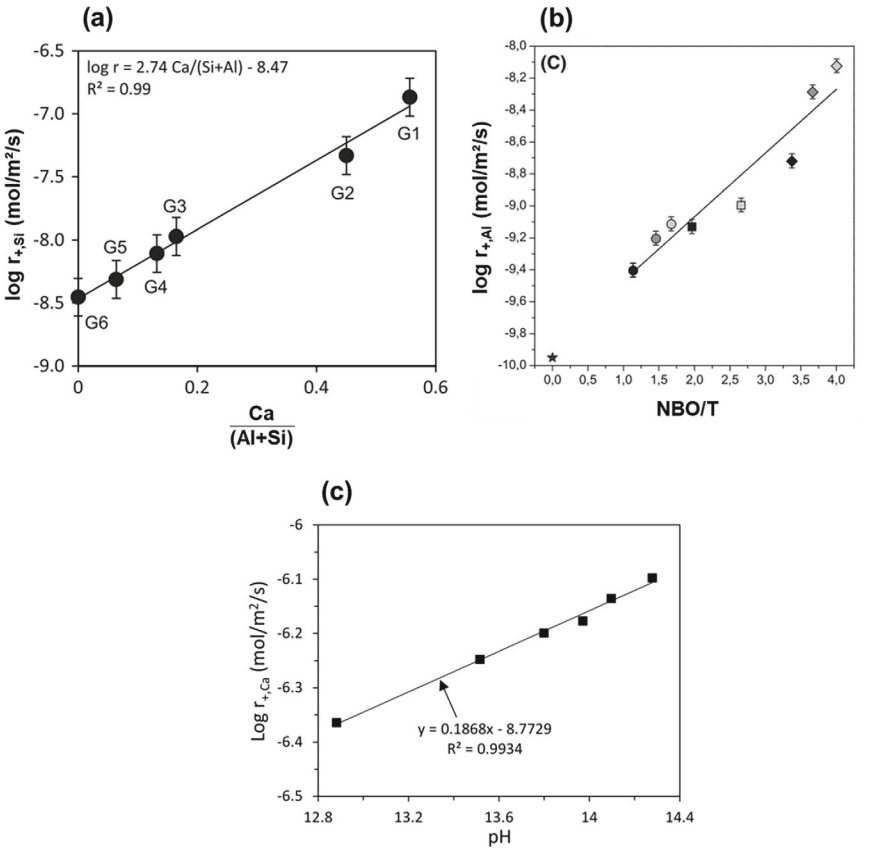

Fig. 11 Influence of the content of CaO of synthetic glasses on dissolution kinetics **a** forward dissolution rate of Si (adapted from [137]) and **b** forward dissolution rate of Al (adapted from [110]); **c** influence of pH on dissolution rate of Ca in commercial slag. (Adapted from [138], Author's copyright)

Therefore, the more significant release of Ca and Al in the initial moments of reaction in slags, compared to fly ashes (assuming that the activator is already supplying the necessary Si), is expected to result in a quicker supersaturation of the pore solution with respect to binding phases, and consequently to promote faster precipitation of these phases. It is of course important to balance the different reaction rates to enable setting and hardening to take place within a desirable timeframe; reactions that are either too slow or too fast give inconvenient behavior when considering practical use of a cement or concrete. The tailoring of the relationship between activators and precursors enables this balance to be achieved in a robust and now relatively well-understood manner.

Among the many conventional experimental techniques that are available in the laboratory, the use of isothermal calorimetry provides a good measurement of the

chemical reactivity of a system, due to the exothermic characteristics of both dissolution and phase precipitation reactions. In such tests, the measurement of the heat release of alkali-activated pastes forms an initial high-intensity peak, attributed to the initial breakdown of the framework of the precursor [140]. This initial period is usually followed by an acceleration stage, which is typical of the initial precipitation of reaction products [105, 141, 142]. Therefore, the analysis of the cumulative heat release of pastes tested under similar conditions, at different ages, can provide a direct comparison regarding the evolution of the reaction in different systems.

The visualization of the reaction evolution using in-situ calorimetry was well illustrated by Sun and Vollpracht [143], who compared the first 48 h of reaction of pastes activated with NaOH and measured a cumulative heat release up to 10 times higher in slag-based systems compared to fly ash ones see Fig. 12a, b. It is interesting to mention that these higher cumulative values are measured despite the fact that the maximum heat flow intensity was obtained in one of the fly ash-pastes. Moreover, it is easy to notice that higher molarities of NaOH (denoted by the numbers in the arrows attached to each curve) increased the final heat release, as the reactivity of AAMs are normally enhanced by higher alkalinities up to a certain extent—it has been claimed that, above threshold values around 8 mol/L, the high concentration of activator retards the reaction process at later stages [92, 141, 144].

With respect to the activation of metakaolin, Zhang et al. [145] observed the absence of a significant acceleration stage in NaOH solutions of 12 mol/L at 20 °C. However, it is interesting to point that, at 40 °C, the same mixtures presented the formation of two acceleration stages, credited to a structural reorganization of initial formed N–A–S–H type gels into zeolite-like crystals see Fig. 12c. The reaction has also been observed to be delayed in sodium silicate solutions [146], directly proportional to the silicate modulus of the activator. At a SiO_2/Na_2O ratio of 1.6, the acceleration peak was either absent (at 25 °C) or significantly less intense (at 40 °C), resulting in a reduction of the overall degree of reaction by approximately 40% when compared to a modulus of 1.0.

The faster reaction of high-Ca precursors has a direct influence on the strength development of AAMs. For instance, Deir et al. [147] found that slag-based pastes, activated with waterglass and cured for 1 day at 50 °C, achieved approximately 2.5 and 2.8 times higher compressive strength values than pastes made with calcareous and siliceous fly ashes, respectively, under similar conditions. Moreover, the authors reported that, for a same silicate modulus, increasing Na_2O content led to the formation of calcium aluminosilicate hydrate gels C–(A–)S–H type gels with higher Ca/Si ratios in slag-based pastes. In a similar trend, Le Saout et al. [23], verified a change in Ca/Si ratio from 0.89 to 0.82 in one day old alkali-activated slag pastes, when activated with NaOH and waterglass respectively, while the degree of hydration decreased from 47 to 41%.

Al has also been shown to directly influence the phase assemblage of mortars and pastes made with synthetic glasses after the first days of reaction, particularly increasing the formation of AFm phases [100, 148]. In the same works, the Si/Al ratio of N–A–S–H gel has been found to follow the initial element ratios in a quasi-linear trend in low-Ca systems, as the NaOH-activation of sodium aluminosilicate synthetic

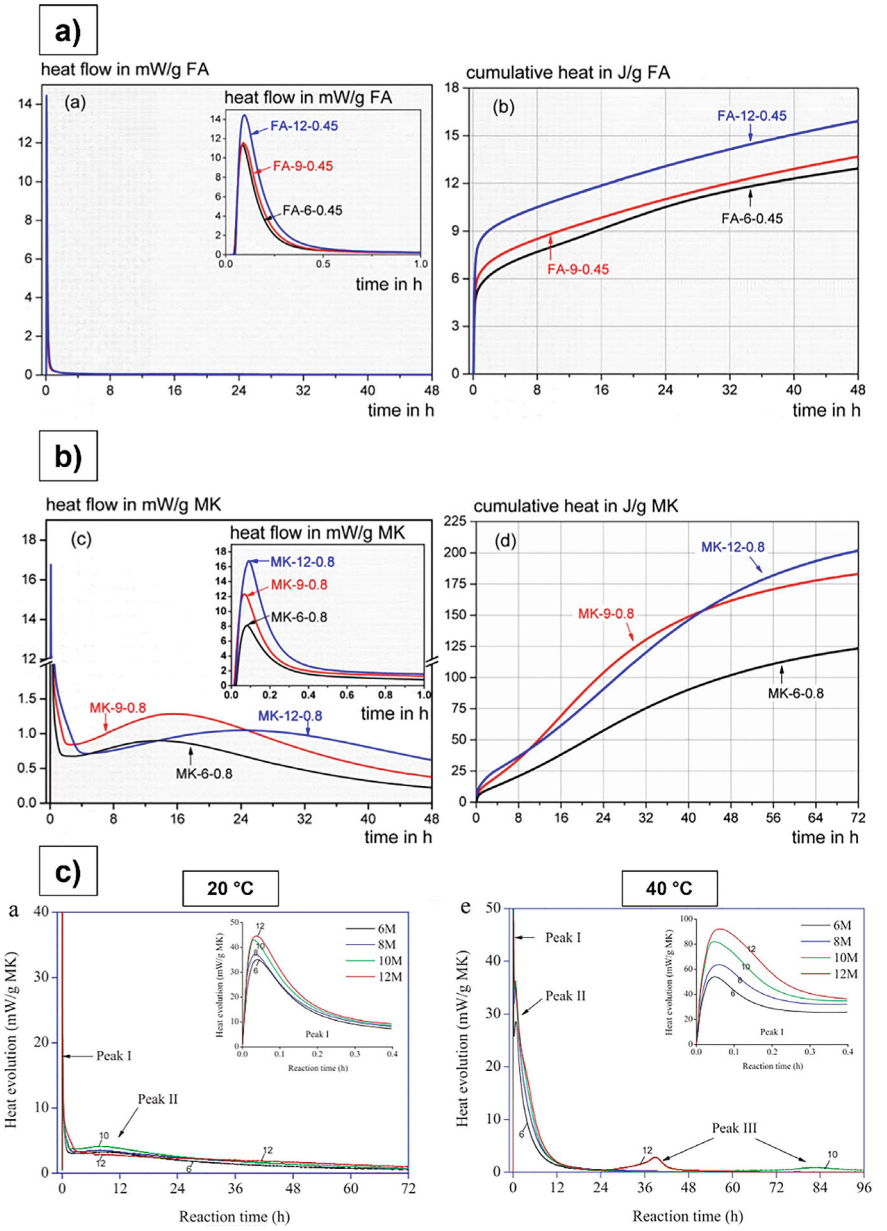

Fig. 12 Effect of the concentration of NaOH in the reaction kinetics of **a** alkali-activated fly ash and **b** alkali-activated slag, using in-situ isothermal calorimetry (adapted from [143], copyright Elsevier), and **c** alkali-activated fly ash at 20 and 60 °C. Adapted from [145], copyright Elsevier

glasses reached final ratios of 1.7 and 5.3 after 20 h of curing at 80 °C (initial element ratios of 2.0 and 6.3, respectively). With respect to sodium silicate activation of fly ash (Ms = 0.79), Provis and van Deventer [149] observed more significant changes in the Si/Al ratios of reaction products in early stages using mathematical modelling and in-situ energy dispersive X-ray diffractometry. The authors reported a reduction of the Si/Al ratio of amorphous gels by the attachment of Al-species in the first 90 min of reaction (reduction from approx. 4.0 to 1.0), while Singh and Subramaniam [150] observed an evolution in the presence of Si content of the gels with time regardless of curing temperatures. With the aid of SEM and EDS, the authors calculated an increase of the Si/Al ratios from approx. 2.0 to 3.5 from 1 to 14 days by the slow incorporation of aqueous silicate species, with negligible changes taking place at longer ages.

Another influencing factor is the choice of the activator type, which influences greatly the type and amount of reaction products forming in the cementitious matrix. Lloyd et al. [151] were among the first ones to observe differences in the nucleation and growth mechanisms of fly ashes activated in different alkaline media. The authors reported a much less uniform microstructure in NaOH-activated when compared to waterglass-activated materials, as the less dense characteristic of the matrix in the former allows an outward growth of initially precipitated units of N–A–S–H type gel. Recently, Sun et al. [83] compared the differences in the development of yield stress in alkali-activated slags using NaOH and waterglass as activators, using in-situ SEM to observe the evolution of the microstructure in different media. The author found that, in waterglass-activated systems, the prompt availability of dissolved silicate species allowed the formation of a less flocculated system with smaller solid crystallites homogeneously distributed in the matrix, while NaOH favored more rapid precipitation of C–A–S–H gel and hydrotalcite, anchored in the precursor surface forming thick rim products—see the sketch in Fig. 13.

3.4 Microstructure and Reaction Products

The differences in reaction kinetics have a direct influence in the type and quantity of the reaction products present in the final microstructure of AAMs. In summary, the hydrated gels to be formed can be categorized in two main groups according to the role of Ca, as schematically illustrated in Fig. 14. In Ca-rich systems, Ca acts as both anchor for nucleation of CaO sheets surrounding silicate chains with variable level of Al^{IV} substitution, and as charge compensator of $[AlO_4]^-$ sites along with other alkaline species (C–(N–A–)S–H type gel) [2, 3]. The C–(N–A–)S–H type gel is described in the literature as a low-order version of tobermorite, which is one of the crystalline analogues used to describe the structure of C–S–H, with alternate layers of CaO and finite silicate chains [16, 152]. C–(N–A–)S–H-type gel displays lower Ca content (showing usually a Ca/Si ratio of around 1.0) and higher Al content (with Al/Si ratio in the range of 0.1–0.2) than C–S–H formed by Portland cement hydration [16, 152–154]. In systems containing low-Ca precursors, Ca is either incorporated

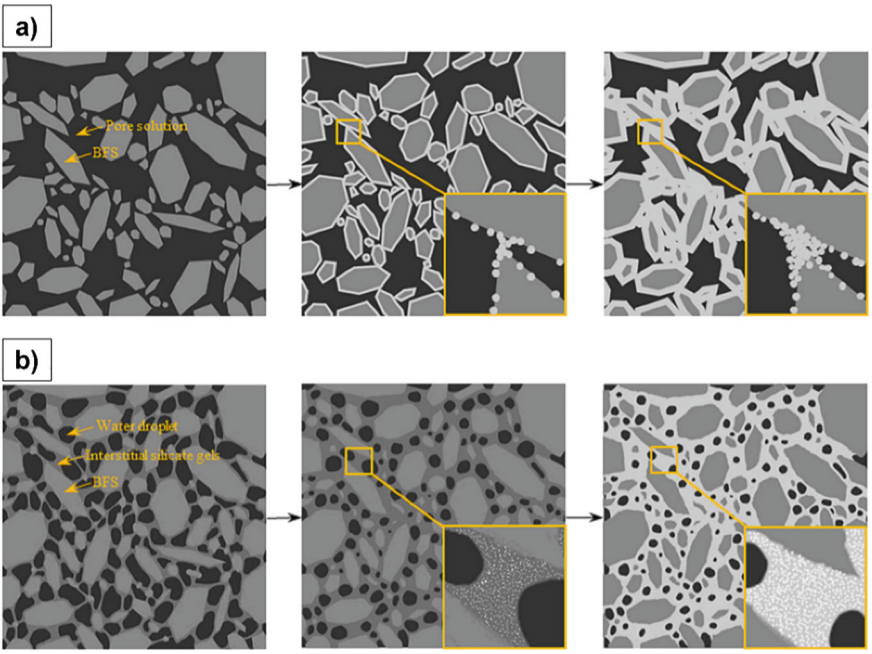

Fig. 13 Schematic illustration of the distribution of crystallites formed in the initial moments of reaction of alkali-activated slag in: **a** sodium hydroxide media; and **b** sodium silicate media (the reaction products are represented with grey dots). Adapted from [83], copyright Elsevier

in N/K–A–S–H type gels [27, 82] as charge balancing species forming N/K–(C–)A–S–H gels, or it is consumed to form secondary reaction products. The N/K–(C–)A–S–H gels can be considered a zeolite-precursor product, presenting similar chemical composition to this class of minerals and structural arrangement limited to short-range order, as reported using X-ray pair distribution functions [155, 156].

The distinction between the Ca-rich and other gels is hard to achieve via most analytical techniques, as the hardened cementitious matrix is composed of an intimate mixture of different reaction products, most of which lack crystalline ordering. A few authors have implemented phase segmentation through chemical analysis [92, 142, 157–162], which has showed to be helpful in the separation of the main gel phases from secondary reaction products. With respect to hydrated gels, the nano-scale volume of each one imposes extra challenges, as they are usually intermixed forming agglomerated regions composed of several gels with different chemical compositions.

The implementation of selective dissolution based on a combination of salicylic acid and methanol (SAM), suggested initially by Takashima [163], can be used on an attempt to quantify the amount of each gel. This treatment is considered suitable for the dissolution of Ca-containing structures, such as C–S–H, C–A–S–H and C–N–A–S–H. After long curing periods, SAM dissolution has been successfully used for the

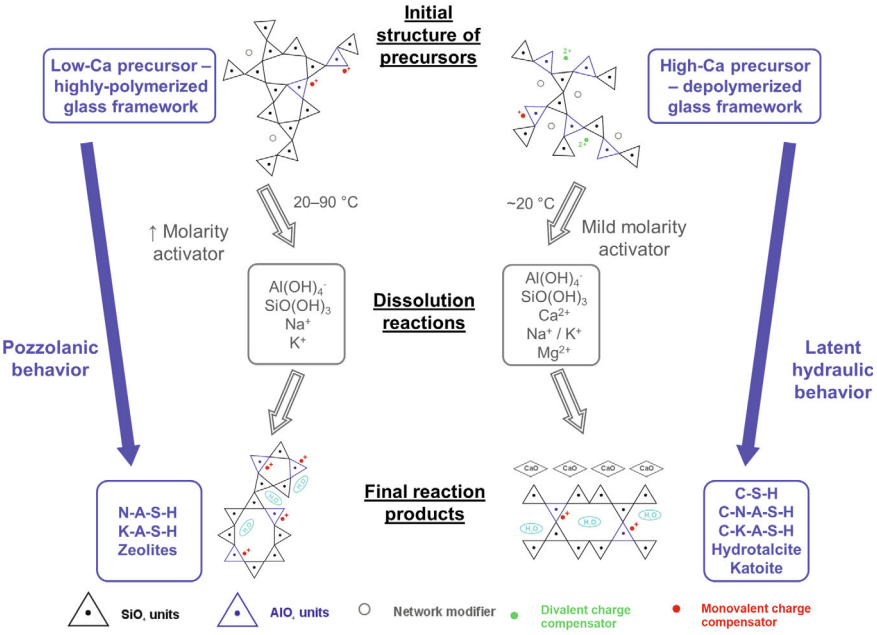

Fig. 14 Conceptual model of alkali-activation of low- and high-Ca precursors. Flowchart adapted from [27]

qualitative study and quantification of N–A–S–H and N–(C–)A–S–H gels in alkali-activated blends of slag and fly ash [161, 164]. By combining phase segmentation of SEM images, quantitative X-ray diffraction and selective dissolution, Miranda de Lima [45] established a correlation between the quantitative determination of variations of C–S–H and N–A–S–H gels—see Fig. 15. The authors analyzed 18 different comprised of synthetic glasses resembling slags and fly ashes, and proposed empirical *phase assemblage indices* which estimate the final quantity of both classes of gels, accounting for chemistry of the precursor, activator, and curing temperature. Equations (3a) and (3b) have been defined for the estimation of C–(N–A–)S–H and N–A–S–H gels, respectively. The colors of the data points indicate pastes made with individual precursors cured at 20 and 60 °C, and pastes made with blended precursors cured at 20 °C.

$$\mathrm{C-(N-A-)S-H}\,index = \frac{\mathrm{Ca+Si}}{\mathrm{Ca+Si+Al+Na}} \cdot \frac{\mathrm{Ca}}{\mathrm{Na}} \cdot \frac{\mathrm{Ca+Si+Al}}{\mathrm{Ca+Si+Al+Na}} \tag{3a}$$

$$\mathrm{N-A-S-H}\,index = \frac{\mathrm{Si}_{precursor}+\mathrm{Al}}{\mathrm{Ca+Si}_{precursor}+\mathrm{Al+Na}} \cdot \frac{\mathrm{Na}}{\mathrm{Ca}} \cdot \frac{\mathrm{Si}_{all}}{\mathrm{Ca}} \cdot \frac{\mathrm{Si}_{all}}{\mathrm{Si}_{precursor}} \cdot \frac{T}{T_{ref}} \tag{3b}$$

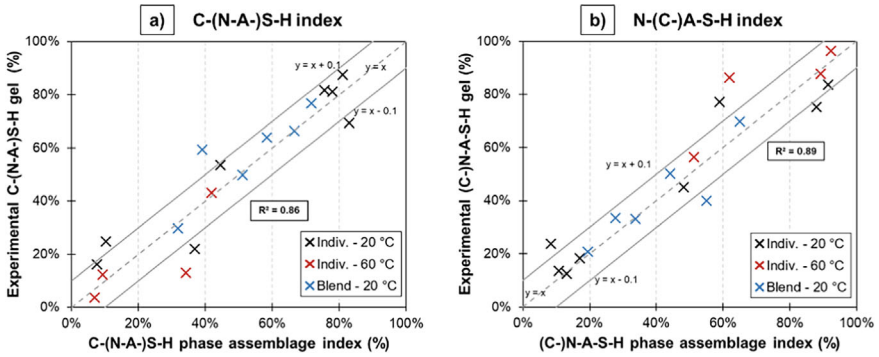

Fig. 15 Correlation of the nucleation indices proposed by Miranda de Lima et al. with the quantitative (wt.%) formation of different categories of hydrated gels: **a** C–(N–A–)S–H gels; and **b** N–A–S–H gels. The indices indicated in the abscissa were defined by the normalized of each one to their sum. Image from Ref. [45], Author's copyright

The formation of secondary reaction products is expected in both classes of precursors, contributing to up to 15% of the volume of the final microstructure [6, 142]. Similarly to what is observed in the hydration of Portland cement, these phases are influenced by the presence of secondary oxides and, specifically in AAMs, by curing conditions and alkalinity of the solution [6–8]. The bulk composition of such precipitates is usually out of the chemical composition stability domain range of pure gels. The two main secondary products are a Mg−, Al-rich lamellar structure, and AFm-like phases [16, 165]. The Mg–Al layered double hydroxide (LDH), a hydrotalcite-resembling phase composed by alternate layers of brucite-like and gibbsite-like units, is usually formed as a rim product during the initial stages of dissolution due to the low mobility of Mg, consuming the majority of Mg atoms supplied by the precursor [151, 153, 166, 167]. However, it is only observed with an MgO content above 5% [16, 168]. A few authors have also reported that varying levels of MgO will not show effect on the chemical composition of C–(N–)A–S–H, thus proving its functionality only as LDH forming agent [169, 170]. The second most important secondary precipitates are AFm-like phases, in which the structure is similar to a layered double hydroxide but the main layer is based on portlandite rather than brucite, with anions providing charge-balancing conditions on the second layer [169].

The main secondary reaction products in low-Ca systems are zeolites. These compounds form a group of crystalline materials with similar chemical composition to N/K–A–S–H gels but with a highly connected tetrahedral aluminosilicate network, displaying a microporous structure with high surface area [171, 172]. Due to their similarity, N/K–A–S–H gels are considered nano-structured zeolite-like species which will not display a full crystallization behavior due to short-term curing conditions and/or the absence of the water or space needed to enable full crystallization [173]. The type of zeolite to be nucleated is highly dependent on parameters of the reaction, such as H_2O/SiO_2 and $OH-/SiO_2$ ratios, amount of cations, Si/Al ratio, and

SiO_2/Na_2O ratio [173]. Formation of a wide range of zeolite types has been reported in the literature, and the catalogue of such phases is vital for a proper understanding of nucleation mechanisms of reaction products and their performance during the application AAMs.

The current state-of-the-art leads to the conclusion that, within all stages of alkali-activating reactions, many factors can have an immediate impact in the microstructure and properties of these binders. Characteristics such as the nature of precursors, the concentration of activators, or curing conditions, should be carefully considered when tailoring mixtures aiming specific applications, as they impose a great influence over the precipitation reaction products and, consequently, performance and service life of AAMs. The great environmental advantages of these systems, and their high potential to be regarded as a solution for a sustainable future of the building industry, combine to strong motivating factors for in-depth studies of their reaction mechanisms, solving the existing knowledge gaps and maximizing the application potential of these binders.

4 One-Part Alkali-Activated Systems

In recent years, the development of one-part or "just add water" alkali-activated cements (AACs) has gained significant attention [174]. One-part AACs are prepared by combining a solid aluminosilicate precursor and a solid alkaline activator to produce a powder that hardens once in contact with water. In practice, fine and coarse aggregates are added to the mix to produce dry-mix mortar or concrete, but this section focuses on the binder part of the mix. Consequently, it is considered that their primary advantage over conventional (or 'two-part') AACs is avoiding the practical difficulties and hazards associated with the handling of strongly alkaline solutions. One-part AACs are therefore considered to be particularly suitable for situations where it is difficult to handle large volumes of alkaline solutions on site.

Historically, one-part AACs are as old as the alkali activation concept itself [175]. The earliest patents related to alkali activation by Whiting in 1895 [176], Kühl in 1908 [177], and Purdon in 1940 [178] all used one-part mixes. Since then, many combinations of precursors and activators have been investigated in the pursuit of manufacturing one-part AACs. This includes combinations of conventional precursors (i.e. fly ash, blast furnace slag, metakaolin) and conventional activators (i.e. solid alkali hydroxides and alkali silicates), as well as a rapidly growing range of unconventional precursors (e.g. other metallurgical slags) or activators (e.g., highly alkaline biomass ashes or red mud) [179]. The scientific literature of one-part AACs has been reviewed extensively in [174, 180], and aspects related to one-part alkali-activated concretes is discussed in [175]. This section focuses on giving an overview of the manufacturing routes of one-part AACs. The feasible manufacturing routes for one-part AACs are largely dependent on the properties of the starting materials including: the reactivity of the precursor(s), and the dissolution kinetics of the activator(s). For this reason, a brief overview will be given for the different manufacturing routes,

describing which combinations of precursors and activators have been used for each route. This will be followed by a summary of the open questions and challenges in the future development of one-part AACs.

4.1 Routes for Producing One-Part Alkali-Activated Cements

Three main routes have been used for production of one-part AACs, and they are summarized in Fig. 16.

Dry-Mixing Precursor and Activator

Dry-mixing is the simplest route—the precursor and solid activator are dry-mixed, before adding water. This is attractive in its simplicity, as it does not require any additional processes beyond the mixing itself. Conventional activators have been used in dry-mixing, for example: sodium silicate in solid form, dry-mixed with a metakaolin precursor [181], waste clay brick powder blended with fly ash and slag [182], and a combination of sodium hydroxide and sodium silicate, dry-mixed with fly ash [183]. While alkali hydroxide and alkali silicate activators may be feasible to use for one-part AACs in laboratory studies, they do not necessarily fulfil the conditions for industrial use. Given that they are highly hygroscopic under typical atmospheric conditions, their shelf life cannot be guaranteed unless effectively sealed [184]. By comparison, ground granulated blast furnace slags are suitable for activation by solid activators that are more stable under typical atmospheric conditions, such as sodium carbonate [185]. However, given that an aqueous solution of sodium carbonate can provide only slow strength development for the binder, there is limited added benefit of a one-part approach. Furthermore, the use of such a one-part approach for GGBS does not resolve the challenges for non-hydraulic precursors. A potential pitfall of using novel solid activators in dry-mixed systems is that they simply do not generate

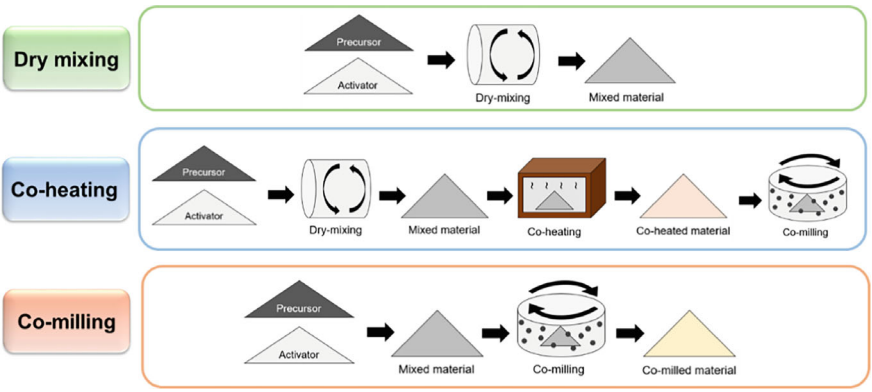

Fig. 16 Routes for one-part alkali-activated cements manufacturing. Adapted from [180]

sufficiently high pH values once the water is added. For instance, this was the case for a blend of 70% fly ash with an addition of 30% olive biomass ash as the intended activator [186]. In contrast, sodium-rich dust (pH = 13.3) produced during a steelmaking process showed promising effects when used to activate GGBS [187].

Solid sodium and magnesium sulfate in conjunction with solid potassium hydroxide was treated as a "greener" route to activate precursors composed of natural kaolin blended with raw ceramic powder [188]. However, a more promising alternative combination is the use of sodium aluminate as a solid activator. This has been used with amorphous silica precursors, including rice husk ash [189], geothermal silica [190], silica fume and filter cake residue from chlorosilane production [191].

Co-heating Precursor and Activator

By heating an aluminosilicate precursor and activator at a sufficiently high temperature, it is possible to produce a partly amorphous material that can be highly soluble in water. In some ways, this route can be considered as manufacturing reactive glasses. This route is also sometimes referred to as "alkali fusion" and is the most well-explored process for synthesis of one-part AACs so far. Co-heating is typically used to valorize precursors which have low reactivity in their as-received form [175]. Naturally occurring minerals, such as feldspars [192] and clays [193], have been popular precursors to use in this route, to increase the amorphous content. Red mud has also been co-heated with sodium hydroxide [194].

Hydrothermal curing is a new and limited-explored direction within this route. Gold mine tailings (comprising mainly quartz, albite, microcline and muscovite) have been hydrothermally activated with sodium hydroxide, and then blended with blast furnace slag [195]. Air pollution control residue (a highly alkaline waste containing 38.3% of Na_2O content by mass) [196] and flue gas residues [197] were investigated as activators as a partial replacement of sodium silicate. The feasibility of activators based on Ca–Mg oxides, which were prepared from dolomite, limestone quarry dust and calcite by calcination, was also confirmed [198].

Blast furnace slag blended with sodium hydroxide could produce one-part alkali-activated slag cements after microwave-treatment [199]. An advantage of this process is that it is more flexible to a range of activators. Milling is necessary as a subsequent processing step, as sintering typically occurs during the heating process. Compared with the dry-mixing route, a disadvantage of co-heating is that it adds two additional process steps: the heating, and subsequent grinding. Another drawback is that co-heating requires sufficiently high temperatures to achieve melting of the solid constituents—this is typically in the range of 800–1200 °C, and for clays that ranges between 600 and 950 °C depending on the types of clay [180].

Co-milling Precursor and Activator

Co-milling involves intensive milling of precursor(s) and activator(s). This approach is based on mechano-chemistry [200] the rationale is to introduce alkali metal cations into the structure of an aluminosilicate precursor [201], while simultaneously increasing structural disorder, decreasing particle size, and increasing reactive surface area of the solid precursor. Those factors then lead to increased rates of

dissolution, and also provide the species in solution necessary to form binder phases. Milling is typically conducted with a ball mill for which the amount of balls, their size distribution, the milling time, rotation speed of the mill, and use of milling admixtures are important parameters [202].

Fly ash has been co-milled with additions of CaO, MgO and NaOH [201], and sodium silicate [203]. The reactivity of fluidized bed combustion (FBC) ash could be increased via milling in alkali activation [204]. Rice husk ash was also used as a partial precursor in slag-based mechano-chemically activated geopolymer [205]. Milling is also applied for improving clay mineral reactivity [206]. Avoiding high temperature treatments is attractive in principle, but there is uncertainty around how scalable these intensive milling processes are. More energy-efficient alternatives to ball mills could be vertical roller mills, which are used on industrial scale [206]. However, it remains largely unknown how the embodied energy of high energy milling compares to that of heating processes at a laboratory scale or industrial scale. Furthermore, the use of aggressive substances in milling is likely to enhance degradation of milling equipment.

A summary of which combinations of precursor(s) and activators have been used for these three routes is given in Table 2. This is not intended to be exhaustive, but gives an indication of the variety of systems trialled for each route.

4.2 Mechanical Properties of One-Part AACs

The mechanical properties of AACs are largely determined by the quantity and type of reaction products forming, and the porosity developed by the material as curing progresses. These factors are in turn influenced by a range of parameters relating to the activator, precursors, mix design and curing regime [27]. For one-part AACs, all these factors still apply, with the added variable of production route. The understanding of one-part AACs' mechanical properties has mostly been limited to compressive strength of cement pastes and mortars [180]. Nonetheless, some meaningful comparisons can be made between one-part and two-part systems produced by the dry-mixing route, when other variables are controlled for. For various combinations of conventional activators (i.e. blast furnace slag, fly ash and metakaolin) and conventional activators (i.e. sodium silicate, sodium hydroxide), one-part AACs consistently exhibit comparable or inferior compressive strength compared to analogous two-part AACs [175, 183, 207–209]. This tendency for one-part AACs to have lower compressive strength has been attributed to slower and less effective dissolution of precursors when dissolution of a solid activator is occurring simultaneously (i.e. in a one-part AAC), compared to when the activator is already fully dissolved (i.e. in a two-part AAC) [209].

Table 2 Examples of precursor and activator combinations used for different manufacturing routes

Dry-mixing			Co-heating			Co-milling		
Precursor	Activator	References	Precursor	Activator	References	Precursor	Activator	References
Rice husk ash	Sodium aluminate	[189, 210]	Sodium feldspar	Sodium hydroxide/ sodium silicate	[192]	Fly ash	CaO, MgO, NaOH	[201]
Metakaolin	Sodium silicate/ Anhydrous sodium metasilicate	[181, 211]	Bentonite	Sodium hydroxide/ sodium carbonate	[193]	Fly ash	Sodium silicate	[203]
Amorphous silica (chlorosilane filter cake)	Sodium aluminate	[191]	Red mud	Sodium hydroxide	[194]	Slag/fly ash	Sodium silicate	[212]
Fly ash	Sodium hydroxide/ sodium silicate	[183]	Gold mine tailings, blast furnace slag*	NaOH	[195]	Slag/fly ash	Sodium silicate/ sodium hydroxide	[213]
Blast furnace slag/fly ash	Olive biomass ash	[186]	Fly ash	Red mud/ NaOH	[214]	Slag/rice husk ash	Sodium silicate/ sodium hydroxide	[205]
Geothermal silica	Sodium aluminate	[190]	Fly ash/blast furnace slag	Air pollution control residue/ sodium silicate	[196]	Slag/silica fume/ phyllite dust	Sodium silicate	[215]

(continued)

Table 2 (continued)

Dry-mixing			Co-heating			Co-milling		
Precursor	Activator	References	Precursor	Activator	References	Precursor	Activator	References
Fly ash/blast furnace slag/ silica fume	Anhydrous sodium silicate	[216]	Fly ash/blast furnace slag	Flue gas residues/ sodium silicate	[197]	Fluidized bed combustion coal fly ash/conventional coal fly ash	Sodium silicate/ sodium hydroxide/ MgO	[204]
Blast furnace slag	Sodium silicate/ potassium hydroxide/sodium carbonate	[217]	Metakaolin	Ca–Mg oxides	[198]	Blast furnace slag	Paper sludge/ sodium hydroxide	[218]
Waste clay brick powder/ fly ash/slag	Anhydrous sodium silicate	[182, 219]	Blast furnace slag/ microsilica/ Sodium-rich green liquor dregs	Sodium-rich green liquor dregs/sodium metasilicate	[220]			
Natural kaolin/raw ceramic powder	Solid potassium hydroxide/sodium sulfate/magnesium sulfate	[188]	Blast furnace slag	Blast furnace slag/sodium hydroxide	[199]			

* Denotes that the precursor was later added, but was not used in the treatment itself

4.3 Open Questions and Challenges

From the three manufacturing routes, each has advantages and disadvantages. Dry-mixing is the most straightforward method but is limited to a narrow range of precursors and activators. Co-heating provides an effective way to simultaneously increase the reactivity of otherwise low-reactivity precursors whilst simultaneously incorporating an activator. Co-milling aims for the same end as co-heating (i.e. a disordered precursor embedded with alkali metal cations), but achieves this by a different means—high-energy milling. Both co-heating and co-milling have shown promising results, but the capacity for precise control of these processes remains unclear. A common limitation of all these alkali sources is that the release rate of alkalinity when mixed with water cannot be finely controlled.

The growth of one-part AACs must be viewed in context with other developments in AACs. The use of near-neutral salt activators such as sodium carbonate and sodium sulfate are becoming well-established for blast furnace slags [185]—this means that the common critique around the high alkalinity of two-part AACs is no longer universally applied. The greatest value of one-part AAC manufacturing methods is when the reactivity of a low reactivity precursor (e.g. framework aluminosilicates like feldspars) can be increased at the same time as manufacturing a one-part AAC.

Questions of scalability are valid for any innovations in the cementitious materials sector. So far, all known co-heating studies have been performed in static furnaces, at the laboratory scale. Whilst calcination is indeed used in the cement industry, it is not yet known how compatible the co-heating methods and the aggressive alkalinity of the activators are with continuous production in a rotary kiln, and the selection of refractories in the kilns needs careful attention in particular, to avoid expensive damage to equipment. Another issue (common to all routes) is ensuring suitable shelf life under reasonable storage conditions and bagging. Storage conditions can highly affect the performance of a one-part AAC [184].

The large investments needed for heating and milling facilities and need of transportation of various AAC precursors hinders their commercialization. Systems which valorize wastes as both precursors and activators would seem to offer a win–win situation. But this also presents challenges for commercialization, with producers and consumers often wary of using unfamiliar waste streams which are not available in large quantities, and without a guarantee of predictable supply and consistent composition. New technologies and processing equipment should be applied to decrease the large investment costs. For example, smaller and mobile milling [221] and heating units could be used to process precursors and produce locally competitive construction materials.

5 Conclusions

This chapter has summarized the progress that has been made during the past decades in designing, formulating, and understanding the basic chemistry of alkali-activated binder systems. While there still remain many avenues for research and development, particularly in mix optimization to balance performance and environmental footprint at a plausible cost level, it is clear that these materials are now understood and characterized at a well-advanced level in the scientific community. From the basis of this understanding, a detailed discussion of factors that control engineering properties (mechanical, durability, and other aspects) can therefore be developed, and that will be the focus of the subsequent chapters of this State of the Art Report.

References

1. Provis, J.L., Van Deventer, J.S.J.: Alkali activated materials: state-of-the-art report, RILEM TC 224-AAM. Springer Science & Business Media (2013)
2. Li, N., Shi, C., Zhang, Z., et al.: A review on mixture design methods for geopolymer concrete. Compos. Part B Eng. **178**, 107490 (2019)
3. Duxson, P., Fernández-Jiménez, A., Provis, J.L., et al.: Geopolymer technology: the current state of the art. J. Mater. Sci. **42**, 2917–2933 (2007)
4. Ouellet-Plamondon, C., Habert, G.: Chapter 25: Life cycle assessment (LCA) of alkali-activated cements and concretes. In: Handbook of Alkali-Activated Cements, Mortars and Concretes, pp. 663–685. Elsevier Ltd. (2014)
5. Duxson, P., Provis, J.L., Lukey, G.C., van Deventer, J.S.J.: The role of inorganic polymer technology in the development of "green concrete." Cem. Concr. Res. **37**(12), 1590–1597 (2007)
6. Schade, T., Bellmann, F., Middendorf, B.: Quantitative analysis of C–(K)–A–S–H-amount and hydrotalcite phase content in finely ground highly alkali-activated slag/silica fume blended cementitious material. Cem. Concr. Res. **153**, 106706 (2022)
7. Ye, H., Radlińska, A.: Quantitative analysis of phase assemblage and chemical shrinkage of alkali-activated slag. J. Adv. Concr. Technol. **14**, 245–260 (2016)
8. Gong, K., White, C.E.: Impact of chemical variability of ground granulated blast-furnace slag on the phase formation in alkali-activated slag pastes. Cem. Concr. Res. **89**, 310–319 (2016)
9. Ryu, G.S., Lee, Y.B., Koh, K.T., Chung, Y.S.: The mechanical properties of fly ash-based geopolymer concrete with alkaline activators. Constr. Build. Mater. **47**, 409–418 (2013)
10. Aydın, S., Baradan, B.: Effect of activator type and content on properties of alkali-activated slag mortars. Compos. Part B Eng. **57**, 166–172 (2014)
11. Glosser, D., Suraneni, P., Isgor, O.B., Weiss, W.J.: Using glass content to determine the reactivity of fly ash for thermodynamic calculations. Cem. Concr. Compos. **115**, 103849 (2021)
12. Ramanathan, S., Croly, M., Suraneni, P.: Comparison of the effects that supplementary cementitious materials replacement levels have on cementitious paste properties. Cem. Concr. Compos. **112**, 103678 (2020)
13. Chave, T., Frugier, P., Gin, S., Ayral, A.: Glass-water interphase reactivity with calcium rich solutions. Geochim. Cosmochim. Acta **75**, 4125–4139 (2011)
14. Newlands, K.C., Macphee, D.E.: The reactivity of aluminosilicate glasses in cements–effects of Ca content on dissolution characteristics and surface precipitation. Adv. Appl. Ceram. **116**, 216–224 (2017)

15. Garcia-Lodeiro, I., Aparicio-Rebollo, E., Fernández-Jimenez, A., Palomo, A.: Effect of calcium on the alkaline activation of aluminosilicate glass. Ceram. Int. **42**, 7697–7707 (2016)
16. Myers, R.J., Bernal, S.A., Provis, J.L.: A thermodynamic model for C–(N–)A–S–H gel: CNASH-ss. Derivation and validation. Cem. Concr. Res. **66**, 27–47 (2014)
17. Skibsted, J., Andersen, M.D.: The effect of alkali ions on the incorporation of aluminum in the calcium silicate hydrate (C–S–H) phase resulting from portland cement hydration studied by ^{29}Si MAS NMR. J. Am. Ceram. Soc. **96**, 651–656 (2013)
18. Yip, C.K., Lukey, G.C., Van Deventer, J.S.J.: The coexistence of geopolymeric gel and calcium silicate hydrate at the early stage of alkaline activation. Cem. Concr. Res. **35**, 1688–1697 (2005)
19. Font, A., Soriano, L., de Moraes Pinheiro, S.M., et al.: Design and properties of 100% waste-based ternary alkali-activated mortars: blast furnace slag, olive-stone biomass ash and rice husk ash. J. Clean. Prod. **243**, 118568 (2020)
20. Bakharev, T.: Geopolymeric materials prepared using class F fly ash and elevated temperature curing. Cem. Concr. Res. **35**, 1224–1232 (2005)
21. Winnefeld, F., Leemann, A., Lucuk, M., et al.: Assessment of phase formation in alkali activated low and high calcium fly ashes in building materials. Constr. Build. Mater. **24**, 1086–1093 (2010)
22. Fernández-Jiménez, A., Palomo, A.: Composition and microstructure of alkali activated fly ash binder: effect of the activator. Cem. Concr. Res. **35**, 1984–1992 (2005)
23. Le, S.G., Ben, H.M., Winnefeld, F., et al.: Hydration degree of alkali-activated slags: a ^{29}Si NMR study. J. Am. Ceram. Soc. **94**, 4541–4547 (2021)
24. Puertas, F., Fernández-Jiménez, A., Blanco-Varela, M.T.: Pore solution in alkali-activated slag cement pastes. Relation to the composition and structure of calcium silicate hydrate. Cem. Concr. Res. **34**, 139–148 (2004)
25. Garcia-lodeiro, I., Palomo, A.: Effect of calcium on the alkaline activation of aluminosilicate glass. Ceram. Int. **42**, 7697–7707 (2016)
26. Bernal, S.A., Provis, J.L., Walkley, B., et al.: Gel nanostructure in alkali-activated binders based on slag and fly ash, and effects of accelerated carbonation. Cem. Concr. Res. **53**, 127–144 (2013)
27. Provis, J.L., Bernal, S.A.: Geopolymers and related alkali-activated materials. Annu. Rev. Mater. Res. **44**, 299–327 (2014)
28. Garcia-Lodeiro, I., Fernández-Jimenez, A., Pena, P., Palomo, A.: Alkaline activation of synthetic aluminosilicate glass. Ceram. Int. **40**, 5547–5558 (2014)
29. Moraes, J.C.B., Tashima, M.M., Akasaki, J.L., et al.: Effect of sugar cane straw ash (SCSA) as solid precursor and the alkaline activator composition on alkali-activated binders based on blast furnace slag (BFS). Constr. Build. Mater. **144**, 214–224 (2017)
30. Bashar, I.I., Alengaram, U.J., Jumaat, M.Z., et al.: Engineering properties and fracture behaviour of high volume palm oil fuel ash based fibre reinforced geopolymer concrete. Constr. Build. Mater. **111**, 286–297 (2016)
31. Bernal, S.A., Rodríguez, E.D., Mejia De Gutiérrez, R., et al.: Activation of metakaolin/slag blends using alkaline solutions based on chemically modified silica fume and rice husk ash. Waste Biomass Valoriz. **3**, 99–108 (2012)
32. Liu, Y., Shi, C., Zhang, Z., Li, N.: An overview on the reuse of waste glasses in alkali-activated materials. Resour. Conserv. Recycl. **144**, 297–309 (2019)
33. Maldonado-Alameda, A., Giro-Paloma, J., Svobodova-Sedlackova, A., et al.: Municipal solid waste incineration bottom ash as alkali-activated cement precursor depending on particle size. J. Clean. Prod. **242**, 118443 (2020)
34. Nguyen, H.T., Hoa, N.N., Vu, D.T., Kien, P.T.: Properties of geopolymer from coal bottom ash and water glass solution. In: Proceedings of RSCE2016 (2016)
35. Bignozzi, M.C., Barbieri, L., Lancellotti, I.: New geopolymers based on electric arc furnace slag. Adv. Sci. Technol. **69**, 117–122 (2010)
36. Garcia Lodeiro, I., Cristelo, N., Palomo, A., Fernández-Jiménez, A.: Use of industrial by-products as alkaline cement activators. Constr. Build. Mater. **253**, 119000 (2020)

37. Buchwald, A., Vanooteghem, M., Gruyaert, E., et al.: Purdocement: application of alkali-activated slag cement in Belgium in the 1950s. Mater. Struct. Constr. **48**, 501–511 (2015)
38. Pacheco-Torgal, F., Castro-Gomes, J., Jalali, S.: Alkali-activated binders: a review. Part 1. Historical background, terminology, reaction mechanisms and hydration products. Constr. Build. Mater. **22**, 1305–1314 (2008)
39. ASTM International.: ASTM C618-19: standard specification for coal fly ash and raw or calcined natural pozzolan for use in concrete. ASTM Stand (2019)
40. BSI.: Methods of testing composition, specifications and conformity criteria for common cements. BSI Stand Publ 50 (2011)
41. Thomas, M.D.A.: Optimizing the use of fly ash in concrete. Portl. Cem. Assoc. **24** (2007)
42. Heidrich, C., Feuerborn, H., Weir, A.: Coal combustion products : a global perspective, p. 12. VGB PowerTech (2013)
43. Hardjito, D., Rangan, B.V.: Development and properties of low-calcium fly ash based geopolymer concrete. Faculty of Engineering Curtin University of Technology. Aust, Univ Technol Perth (2005)
44. Li, C., Li, Y., Sun, H., Li, L.: The composition of fly ash glass phase and its dissolution properties applying to geopolymeric materials. J. Am. Ceram. Soc. **94**, 1773–1778 (2011)
45. Miranda de Lima, L.: Temperature-chemistry-microstructure correlations for alkali-activated binders. Delft University of Technology, Faculty of Civil Engineering and Geosciences (2025)
46. Alengaram, U.J.: Valorization of industrial byproducts and wastes as sustainable construction materials. In: Handbook of Alkali-Activated Cements, Mortars and Concretes, pp. 23–43. Elsevier Ltd. (2021)
47. Kim, H.K.: Coal bottom ash. In: Sustainable Concrete Made with Ashes and Dust from Different Sources, pp. 29–59. Elsevier Ltd. (2021)
48. Hemmings, R.T., Berry, E.E.: On the glass in coal fly ashes: recent advances. MRS Proc. **113**, 3–38 (1987)
49. Wei, G., Dong, B., Fang, G., Wang, Y.: Understanding reactive amorphous phases of fly ash through the acidolysis. Cem. Concr. Compos. **140**, 105102 (2023)
50. Sarabèr, A.: Co-combustion and its impact on fly ash quality; pilot-scale experiments. Fuel Process. Technol. **104**, 105–114 (2012)
51. Wu, M.F., Huang, W.H.: Evaluation of fly ash from co-combustion of paper mill wastes and coal as supplementary cementitious materials. Materials **15**, 8931 (2022)
52. Faleschini, F., Zanini, M.A., Brunelli, K., Pellegrino, C.: Valorization of co-combustion fly ash in concrete production. Mater. Des. **85**, 687–694 (2015)
53. Kearney, S., Yorkshire, A.S., Geddes, D.A., et al.: Cement-based stabilization/solidification of radioactive waste. In: Low Carbon Stabilization and Solidification of Hazardous Wastes, pp. 407–431 (2021)
54. Dones, R., Heck, T.: Greenhouse gas emissions from energy systems. Encycl. Energy **3**, 77–95 (2004)
55. World Steel Association.: Steel facts (2018)
56. Wang, G.C.: Ferrous metal production and ferrous slags. In: The Utilization of Slag in Civil Infrastructure Construction, pp. 9–33 (2016)
57. Kokal, H.R., Ranade, M.G.: Fluxes for Metallurgy. Industrial Minerals and Rocks, pp. 661–675
58. Pal, S.C., Mukherjee, A., Pathak, S.R.: Investigation of hydraulic activity of ground granulated blast furnace slag in concrete. Cem. Concr. Res. **33**, 1481–1486 (2003)
59. Darquennes, A., Espion, B., Staquet, S.: How to assess the hydration of slag cement concretes? Constr. Build. Mater. **40**, 1012–1020 (2013)
60. Zhang, Y., Zhang, S., Chen, Y., Çopuroğlu, O.: The effect of slag chemistry on the reactivity of synthetic and commercial slags. Constr. Build. Mater. **335**, 127493 (2022)
61. De Belie, N., Soutsos, M., Gruyaert, E.: Properties of Fresh and Hardened Concrete Containing Supplementary Cementitious Materials: State-of-the-Art Report of the RILEM Technical Committee 238-SCM, Working Group 4. Springer Science & Business Media (2018)

62. Rehackova, L., Rosypalova, S., Dudek, R., et al.: Effect of CaO/SiO2 ratio on viscosity and structure of slag. Metallurgija **54**, 455–458 (2015)
63. Fisher, L.V., Barron, A.R.: The recycling and reuse of steelmaking slags—A review. Resour. Conserv. Recycl. **146**, 244–255 (2019)
64. Khorshidi, Z.N., Tan, X., Liu, Q., Choi, P.: Molecular dynamics study of the dissolution mechanism of kaolinite basal surfaces in alkali media. Appl. Clay Sci. **152**, 29–37 (2018)
65. Hanein, T., Nguyen, H., Provis, J.L., et al.: Thermodynamics of calcined clays used in cementitious binders: origin to service life considerations. J. Mater. Chem. A **11**, 17920–17937 (2023)
66. Fernandez, R., Martirena, F., Scrivener, K.L.: The origin of the pozzolanic activity of calcined clay minerals: a comparison between kaolinite, illite and montmorillonite. Cem. Concr. Res. **41**, 113–122 (2011)
67. White, C.E., Provis, J.L., Proffen, T., et al.: Combining density functional theory (DFT) and pair distribution function (PDF) analysis to solve the structure of metastable materials: the case of metakaolin. Phys. Chem. Chem. Phys. **12**, 3239–3245 (2010)
68. Rocha, J., Klinowski, J.: 29Si and 27Al magic-angle-spinning NMR studies of the thermal transformation of kaolinite. Phys. Chem. Miner. **17**, 179–186 (1990)
69. Longhi, M.A., Rodríguez, E.D., Bernal, S.A., et al.: Valorisation of a kaolin mining waste for the production of geopolymers. J. Clean. Prod. **115**, 265–272 (2016)
70. Sanz, J., Madani, A., Serratosa, J.M., et al.: Aluminum-27 and Silicon-29 magic-angle spinning nuclear magnetic resonance study. J. Am. Ceram. Soc. **421**, 418–421 (1988)
71. Moya, J.S., Cabal, B., Bartolome, J.F., et al.: Significance of the formation of pentahedral aluminum in the reactivity of calcined kaolin/metakaolin and its applications. Ceram. Int. **50**, 1329–1340 (2024)
72. White, C.E., Kearley, G.J., Provis, J.L., Riley, D.P.: Inelastic neutron scattering analysis of the thermal decomposition of kaolinite to metakaolin. Chem. Phys. **427**, 82–86 (2013)
73. Ranjbar, N., Kuenzel, C., Spangenberg, J., Mehrali, M.: Hardening evolution of geopolymers from setting to equilibrium: a review. Cem. Concr. Compos. **114**, 103729 (2020)
74. Assi, L.N., Carter, K., Deaver, E., Ziehl, P.: Review of availability of source materials for geopolymer/sustainable concrete. J. Clean. Prod. **263**, 121477 (2020)
75. Matthys, S., Ghorbani, S., Krajnovic, I., et al.: The Urban Concrete Innovation. Ghent University (2023)
76. Brindley, G.W., Nakahira, M.: A new concept of the transformation sequence of kaolinite to mullite. Nature **181**, 1333–1334 (1958)
77. Khaled, Z., Mohsen, A., Soltan, A.M., Kohail, M.: Optimization of kaolin into Metakaolin: calcination conditions, mix design and curing temperature to develop alkali activated binder. Ain Shams Eng. J. **14**, 102142 (2023)
78. Kim, J.Y., Hwang, K.T.: Properties of kaolinite as a raw material for porcelain. J. Korean Ceram. Soc. **56**, 566–576 (2019)
79. Wang, S., Gainey, L., Mackinnon, I.D.R., Xi, Y.: High- and low-defect kaolinite for brick making: Comparisons of technological properties, phase evolution and microstructure. Constr. Build. Mater. **366**, 130250 (2023)
80. Wetzel, A., Middendorf, B.: Influence of silica fume on properties of fresh and hardened ultra-high performance concrete based on alkali-activated slag. Cem. Concr. Compos. **100**, 53–59 (2019)
81. Duxson, P., Provis, J.L.: Designing precursors for geopolymer cements. J. Am. Ceram. Soc. **91**, 3864–3869 (2008)
82. Garcia-Lodeiro, I., Palomo, A., Fernández-Jiménez, A.: Ch. 2: An overview of the chemistry of alkali-activated cement-based binders. In: Handbook of Alkali-Activated Cements, Mortars and Concretes, pp 19–47. Woodhead Publishing Limited (2015)
83. Sun, Y., de Lima, L.M., Rossi, L., et al.: Interpretation of the early stiffening process in alkali-activated slag pastes. Cem. Concr. Res. **167**, 107118 (2023)
84. Fernández-Jiménez, A., Palomo, A., Criado, M.: Microstructure development of alkali-activated fly ash cement: a descriptive model. Cem. Concr. Res. **35**, 1204–1209 (2005)

85. Palomo, A., Krivenko, P., Garcia-Lodeiro, I., et al.: A review on alkaline activation: new analytical perspectives. Mater. Constr. **64**, 315 (2014)
86. Williamson, T., Juenger, M.C.G.: The role of activating solution concentration on alkali-silica reaction in alkali-activated fly ash concrete. Cem. Concr. Res. **83**, 124–130 (2016)
87. Puertas, F., González-Fonteboa, B., González-Taboada, I., et al.: Alkali-activated slag concrete: fresh and hardened behaviour. Cem. Concr. Compos. **53**, 279–288 (2018)
88. Komkova, A., Habert, G.: Environmental impact assessment of alkali-activated materials: examining impacts of variability in constituent production processes and transportation. Constr. Build. Mater. **363**, 129032 (2023)
89. Palacios, M., Banfill, P.F.G., Puertas, F.P.: Rheology and setting of alkali-activated slag pastes and mortars: effect of organic admixture. ACI Mater. J. **105**, 140–148 (2008)
90. Qing-Hua, C., Sarkar, S.L.: A study of rheological and mechanical properties of mixed alkali activated slag pastes. Adv. Cem. Based Mater. **1**, 178–184 (1994)
91. Douglas, E., Bilodeau, A., Malhotra, V.M.: Properties and durability of alkali-activated slag concrete. Mater. J. **89**, 509–516 (1992)
92. Ravikumar, D., Neithalath, N.: Effects of activator characteristics on the reaction product formation in slag binders activated using alkali silicate powder and NaOH. Cem. Concr. Compos. **34**, 809–818 (2012)
93. Sun, B., Sun, Y., Ye, G., De Schutter, G.: A mix design methodology of slag and fly ash-based alkali-activated paste. Cem. Concr. Compos. **126**, 104368 (2022)
94. Palacios, M., Gismera, S., Alonso, M.M., et al.: Early reactivity of sodium silicate-activated slag pastes and its impact on rheological properties. Cem. Concr. Res. **140**, 106302 (2021)
95. Gebregziabiher, B.S., Thomas, R., Peethamparan, S.: Very early-age reaction kinetics and microstructural development in alkali-activated slag. Cem. Concr. Compos. **55**, 91–102 (2015)
96. Puertas, F., Varga, C., Alonso, M.M.: Rheology of alkali-activated slag pastes. Effect of the nature and concentration of the activating solution. Cem. Concr. Compos. **53**, 279–288 (2014)
97. Provis, J.L., Kilcullen, A., Duxson, P., et al.: Stabilization of low-modulus sodium silicate solutions by alkali substitution. Ind. Eng. Chem. Res. **51**, 2483–2486 (2012)
98. Sun, B., Ye, G., de Schutter, G.: A review: reaction mechanism and strength of slag and fly ash-based alkali-activated materials. Constr. Build. Mater. **326**, 126843 (2022)
99. Shimoda, K., Tobu, Y., Kanehashi, K., et al.: Total understanding of the local structures of an amorphous slag: perspective from multi-nuclear (29Si, 27Al, 17O, 25Mg, and 43Ca) solid-state NMR. J. Non Cryst. Solids **354**, 1036–1043 (2008)
100. Kucharczyk, S., Zajac, M., Stabler, C., et al.: Structure and reactivity of synthetic CaO–Al2O3–SiO2 glasses. Cem. Concr. Res. **120**, 77–91 (2019)
101. Li, G., Zhou, C., Ahmad, W., et al.: Fly ash application as supplementary cementitious material: a review. Materials **15**, 1–23 (2022)
102. Cyr, M., Trinh, M., Husson, B., Casaux-Ginestet, G.: Effect of cement type on metakaolin efficiency. Cem. Concr. Res. **64**, 63–72 (2014)
103. Hannesson, G., Kuder, K., Shogren, R., Lehman, D.: The influence of high volume of fly ash and slag on the compressive strength of self-consolidating concrete. Constr. Build. Mater. **30**, 161–168 (2012)
104. Vollpracht, A., Soutsos, M., Kanavaris, F.: Strength development of GGBS and fly ash concretes and applicability of fib model code's maturity function—A critical review. Constr. Build. Mater. **162**, 830–846 (2018)
105. Suraneni, P., Hajibabaee, A., Ramanathan, S., et al.: New insights from reactivity testing of supplementary cementitious materials. Cem. Concr. Compos. **103**, 331–338 (2019)
106. Bhat, R., Han, T., Akshay Ponduru, S., et al.: Predicting compressive strength of alkali-activated systems based on the network topology and phase assemblages using tree-structure computing algorithms. Constr. Build. Mater. **336**, 127557 (2022)
107. Varshneya, A.K., Mauro, J.C.: Fundamentals of Inorganic Glass Making. Academic Press Inc. (1994)
108. Callister, W.D.: Materials Science and Engineering—An Introduction. Wiley (2007)

109. Mills, K.C., Yuan, L., Jones, R.T.: Estimating the physical properties of slags. J. South African Inst. Min. Metall. **111**, 649–658 (2011)
110. Schöler, A., Winnefeld, F., Ben, H.M., Lothenbach, B.: The effect of glass composition on the reactivity of synthetic glasses. J. Am. Ceram. Soc. **100**, 2553–2567 (2017)
111. Walkley, B., Provis, J.L.: Solid-state nuclear magnetic resonance spectroscopy of cements. Mater. Today Adv. **1**, 100007 (2019)
112. Poe, B.T., Mcmillan, P.F., Cote, B.: SiO2–Al2O3 liquids: in-situ study by high-temperature 27Al NMR spectroscopy and molecular dynamics simulation. J. Phys. Chem. 8220–8224 (1992)
113. Oey, T., Frederiksen, K.F., Mascaraque, N., et al.: The role of the network-modifier's field-strength in the chemical durability of aluminoborate glasses. J. Non Cryst. Solids **505**, 279–285 (2019)
114. Jiusti, J., Zanotto, E.D., Feller, S.A., et al.: Effect of network formers and modifiers on the crystallization resistance of oxide glasses. J. Non Cryst. Solids **550**, 120359 (2020)
115. Fernández-Jiménez, A., Palomo, A.: Characterisation of fly ashes. Potential reactivity as alkaline cements. Fuel **82**, 2259–2265 (2003)
116. Blotevogel, S., Montouillout, V., Canizares, A., et al.: Glass structure of industrial ground granulated blast furnace slags (GGBS) investigated by time-resolved Raman and NMR spectroscopies. J. Mater. Sci. **56**, 17490–17504 (2021)
117. Diamond, S.: On the glass present in low-calcium and in high-calcium fly ashes. Cem. Concr. Res. **13**, 459–464 (1983)
118. McCarthy, G.J., Johase, D.M., Steinwand, S.J., Thedchanamoorthy, A.: X-ray diffraction analysis of fly ash. In: Advances in X-ray Analysis, volume 34: Thirty-ninth Annual Conference on Application X-ray Analysis, vol. 34, pp. 387–394 (1990)
119. Goto, S., Fujimori, H., Hidaka, A., Ioku, K.: Effects of components on the rate of heat liberation of the hydration in the system of glass/gypsum/lime. J. Eur. Ceram. Soc. **26**, 771–776 (2006)
120. Kenne Diffo, B.B., Elimbi, A., Cyr, M., et al.: Effect of the rate of calcination of kaolin on the properties of metakaolin-based geopolymers. J. Asian Ceram. Soc. **3**, 130–138 (2015)
121. Saidi, N., Samet, B., Baklouti, S.: Effect of composition on structure and mechanical properties of metakaolin based PSS-geopolymer. Int. J. Mater. Sci. **3**, 145 (2013)
122. Vogt, O., Ukrainczyk, N., Ballschmiede, C., Koenders, E.: Reactivity and microstructure of metakaolin based geopolymers: effect of fly ash and liquid/solid contents. Materials **12**, 3485 (2019)
123. Kim, B., Lee, S.: Review on characteristics of metakaolin-based geopolymer and fast setting. J. Korean Ceram. Soc. **57**, 368–377 (2020)
124. Fernández-Jiménez, A., Palomo, A.: Mid-infrared spectroscopic studies of alkali-activated fly ash structure. Microporous Mesoporous Mater. **86**, 207–214 (2005)
125. Chancey, R.T., Stutzman, P., Juenger, M.C.G., Fowler, D.W.: Comprehensive phase characterization of crystalline and amorphous phases of a class F fly ash. Cem. Concr. Res. **40**, 146–156 (2010)
126. Jin, Y., Feng, W., Zheng, D., et al.: Structure refinement of fly ash in connection with its reactivity in geopolymerization. Waste Manag. **118**, 350–359 (2020)
127. Ibáñez, J., Font, O., Moreno, N., et al.: Quantitative Rietveld analysis of the crystalline and amorphous phases in coal fly ashes. Fuel **105**, 314–317 (2013)
128. Zhang, Z., Provis, J.L., Zou, J., et al.: Toward an indexing approach to evaluate fly ashes for geopolymer manufacture. Cem. Concr. Res. **85**, 163–173 (2016)
129. Mehta, P.K.: Influence of fly ash characteristics on the strength of Portland-fly ash mixtures. Cem. Concr. Res. **15**, 669–674 (1985)
130. Uchikawa, H., Uchida, S.: Effect of characteristics of glass phase in blending components on their reactivity in calcium hydroxide mixture. In: 8th International Conference on Chemical, vol. 4, pp. 245–250 (1986)
131. Weng, L., Sagoe-Crentsil, K.: Dissolution processes, hydrolysis and condensation reactions during geopolymer synthesis: Part I-Low Si/Al ratio systems. J. Mater. Sci. **42**, 2997–3006 (2007)

132. Rees, C.A., Provis, J.L., Lukey, G.C., van Deventer, J.S.J.: The mechanism of geopolymer gel formation investigated through seeded nucleation. Colloids Surf. A Physicochem. Eng. Asp. **318**, 91–105 (2008)
133. Dupuis, R., Pellenq, R., Champenois, J., Poulesquen, A.: Dissociation mechanisms of dissolved alkali silicates in sodium hydroxide. J. Phys. Chem. C **124**, 8288–8294 (2020)
134. Ramaswamy, R., Yliniemi, J., Illikainen, M.: Dissolution-precipitation reactions of silicate mineral fibers at alkaline pH. Cem. Concr. Res. **160**, 106922 (2022)
135. Sowoidnich, T., Damidot, D., Ludwig, H.M., et al.: The nucleation of C–S–H via prenucleation clusters. J. Chem. Phys. **158**, 114309 (2023)
136. Krautwurst, N., Nicoleau, L., Dietzsch, M., et al.: Two-step nucleation process of calcium silicate hydrate, the nanobrick of cement. Chem. Mater. **30**, 2895–2904 (2018)
137. Snellings, R.: Solution-controlled dissolution of supplementary cementitious material glasses at pH 13: the effect of solution composition on glass dissolution rates. J. Am. Ceram. Soc. **96**, 2467–2475 (2013)
138. Zuo, Y.: Experimental study and numerical simulation of the reaction process and microstructure formation of alkali-activated materials. Delft University of Technology, Faculty of Civil Engineering and Geosciences (2019)
139. Hamdan, A., Hajimohammadi, A., Rawal, A., Kim, T.: The intrinsic role of network modifiers (Ca vs. Mg) in the reaction kinetics and microstructure of sodium silicate-activated CaO–MgO–Al2O3–SiO2 glasses. Cem. Concr. Res. **164**, 107058 (2023)
140. Scrivener, K., Snellings, R., Lothenbach, B.: A Practical Guide to Microstructural Analysis of Cementitious Materials. CRC Press (2016)
141. Chithiraputhiran, S., Neithalath, N.: Isothermal reaction kinetics and temperature dependence of alkali activation of slag, fly ash and their blends. Constr. Build. Mater. **45**, 233–242 (2013)
142. Zuo, Y., Nedeljković, M., Ye, G.: Coupled thermodynamic modelling and experimental study of sodium hydroxide activated slag. Constr. Build. Mater. **188**, 262–279 (2018)
143. Sun, Z., Vollpracht, A.: One year geopolymerisation of sodium silicate activated fly ash and metakaolin geopolymers. Cem. Concr. Compos. **95**, 98–110 (2019)
144. Bilek Jr. V.B., Novotný, R., Koplík, J., Kadlec, M.: Philosophy of rational mixture proportioning of alkali-activated materials validated by the hydration kinetics of alkali-activated slag and its microstructure. Cem. Concr. Compos. **168**, 107139 (2023)
145. Zhang, Z., Wang, H., Provis, J.L., et al.: Quantitative kinetic and structural analysis of geopolymers. Part 1. The activation of metakaolin with sodium hydroxide. Thermochim. Acta **539**, 23–33 (2012)
146. Zhang, Z., Provis, J.L., Wang, H., et al.: Quantitative kinetic and structural analysis of geopolymers. Part 2. Thermodynamics of sodium silicate activation of metakaolin. Thermochim. Acta **565**, 163–171 (2013)
147. Deir, E., Gebregziabiher, B.S., Peethamparan, S.: Influence of starting material on the early age hydration kinetics, microstructure and composition of binding gel in alkali activated binder systems. Cem. Concr. Compos. **48**, 108–117 (2014)
148. Walkley, B., San Nicolas, R., Sani, M.A., et al.: Phase evolution of C–(N)–A–S–H/N–A–S–H gel blends investigated via alkali-activation of synthetic calcium aluminosilicate precursors. Cem. Concr. Res. **89**, 120–135 (2016)
149. Provis, J.L., van Deventer, J.S.J.: Geopolymerisation kinetics. 2. Reaction kinetic modelling. Chem. Eng. Sci. **62**, 2318–2329 (2007)
150. Singh, G.V.P.B., Subramaniam, K.V.L.: Influence of processing temperature on the reaction product and strength gain in alkali-activated fly ash. Cem. Concr. Compos. **95**, 10–18 (2019)
151. Lloyd, R.R., Provis, J.L., Van Deventer, J.S.J.: Microscopy and microanalysis of inorganic polymer cements. 2: the gel binder. J. Mater. Sci. **44**, 620–631 (2009)
152. Taylor, H.F.W.: Nanostructure of CSH: current status. Adv. Cem. Based Mater. **1**, 38–46 (1993)
153. Richardson, I.G., Groves, G.W.: Microstructure and microanalysis of hardened cement pastes involving ground granulated blast-furnace slag. J. Mater. Sci. **27**, 6204–6212 (1992)

154. Puertas, F., Palacios, M., Manzano, H., et al.: A model for the C–A–S–H gel formed in alkali-activated slag cements. J. Eur. Ceram. Soc. **31**, 2043–2056 (2011)
155. Grangeon, S., Fernandez-Martinez, A., Baronnet, A., et al.: Quantitative X-ray pair distribution function analysis of nanocrystalline calcium silicate hydrates: a contribution to the understanding of cement chemistry. J. Appl. Crystallogr. **50**, 14–21 (2017)
156. White, C.E., Provis, J.L., Bloomer, B., et al.: In situ X-ray pair distribution function analysis of geopolymer gel nanostructure formation kinetics. Phys. Chem. Chem. Phys. **15**, 8573–8582 (2013)
157. Kim, T., Moradian, M., Ley, M.T.: Dissolution and leaching of fly ash in nitric acid using automated scanning electron microscopy. Adv. Civil Eng. Mater. **7**, 20180016 (2018)
158. Gao, X., Yu, Q.L., Brouwers, H.J.H.: Apply 29Si, 27Al MAS NMR and selective dissolution in identifying the reaction degree of alkali activated slag-fly ash composites. Ceram. Int. **43**, 12408–12419 (2017)
159. Hu, Z., Wyrzykowski, M., Lura, P.: Estimation of reaction kinetics of geopolymers at early ages. Cem. Concr. Res. **129**, 105971 (2020)
160. Zhu, W., Chen, X., Struble, L.J., Yang, E.H.: Characterization of calcium-containing phases in alkali-activated municipal solid waste incineration bottom ash binder through chemical extraction and deconvoluted Fourier transform infrared spectra. J. Clean. Prod. **192**, 782–789 (2018)
161. García-Lodeiro, I., Fernández-Jiménez, A., Blanco, M.T., Palomo, A.: FTIR study of the sol-gel synthesis of cementitious gels: C–S–H and N–A–S–H. J. Sol-Gel Sci. Technol. **45**, 63–72 (2008)
162. Kuenzel, C., Ranjbar, N.: Dissolution mechanism of fly ash to quantify the reactive aluminosilicates in geopolymerisation. Resour. Conserv. Recycl. **150**, 104421 (2019)
163. Takashima, S.: Systematic dissolution of calcium silicate in commercial Portland cement by organic acid dissolution. In: Review of the 12th General Meeting, pp. 12–13. Japan Cement Engineering Association Tokyo (1958)
164. Puligilla, S., Mondal, P.: Co-existence of aluminosilicate and calcium silicate gel characterized through selective dissolution and FTIR spectral subtraction. Cem. Concr. Res. **70**, 39–49 (2015)
165. Richardson, I.G., Brough, A.R., Brydson, R., et al.: Location of aluminium in substituted calcium silicate hydrate (C–S–H) gels as determined by Si-29 and Al-27 NMR and EELS. J. Am. Ceram. Soc. **76**, 2285–2288 (1993)
166. Damidot, D., Lothenbach, B., Herfort, D., Glasser, F.P.: Thermodynamics and cement science. Cem. Concr. Res. **41**, 679–695 (2011)
167. Myers, R.J., Bernal, S.A., Provis, J.L.: Phase diagrams for alkali-activated slag binders. Cem. Concr. Res. **95**, 30–38 (2017)
168. Lothenbach, B., Matschei, T., Möschner, G., Glasser, F.P.: Thermodynamic modelling of the effect of temperature on the hydration and porosity of Portland cement. Cem. Concr. Res. **38**, 1–18 (2008)
169. Ben Haha, M., Le Saout, G., Winnefeld, F., Lothenbach, B.: Influence of activator type on hydration kinetics, hydrate assemblage and microstructural development of alkali activated blast-furnace slags. Cem. Concr. Res. **41**, 301–310 (2011)
170. Bernal, S.A., Provis, J.L., Rose, V., Mejía De Gutierrez, R.: Evolution of binder structure in sodium silicate-activated slag-metakaolin blends. Cem. Concr. Compos. **33**, 46–54 (2011)
171. Rożek, P., Król, M., Mozgawa, W.: Geopolymer-zeolite composites: a review. J. Clean. Prod. **230**, 557–579 (2019)
172. Ma, B., Lothenbach, B.: Synthesis, characterization, and thermodynamic study of selected Na-based zeolites. Cem. Concr. Res. **135**, 106111 (2020)
173. Criado, M., Fernández-Jiménez, A., Palomo, A.: Alkali activation of fly ash: effect of the SiO2/Na2O ratio. Part I: FTIR study. Microporous Mesoporous Mater. **106**, 180–191 (2007)
174. Luukkonen, T., Abdollahnejad, Z., Yliniemi, J., et al.: One-part alkali-activated materials: a review. Cem. Concr. Res. **103**, 21–34 (2018)

175. Segura, I.P., Luukkonen, T., Yliniemi, J., et al.: Comparison of one-part and two-part alkali-activated metakaolin and blast furnace slag. J. Sustain. Metall. **8**, 1816–1830 (2022)
176. Whiting, J.: Manufacture of cement. United States Pat. Off. 537,404 (1895)
177. Kühl, H.: Slag cement and process of making the same. United States Pat Off 900,939 (1908)
178. Purdon, A.: The action of alkalis on blast-furnace slag. J. Soc. Chem. Ind. **59**(9), 191–202 (1940)
179. Adesanya, E., Perumal, P., Luukkonen, T., et al.: Opportunities to improve sustainability of alkali-activated materials: a review of side-stream based activators. J. Clean. Prod. **286**, 125558 (2021)
180. Elzeadani, M., Bompa, D.V., Elghazouli, A.Y.: One part alkali activated materials: a state-of-the-art review. J. Build. Eng. **57**, 104871 (2022)
181. Hajimohammadi, A., Ngo, T., Mendis, P., et al.: Pore characteristics in one-part mix geopolymers foamed by H2O2: the impact of mix design. Mater. Des. **130**, 381–391 (2017)
182. Migunthanna, J., Rajeev, P., Sanjayan, J.: Investigation of waste clay brick as partial replacement in geopolymer binder. Constr. Build. Mater. **365**, 130107 (2023)
183. Suwan, T., Fan, M.: Effect of manufacturing process on the mechanisms and mechanical properties of fly ash-based geopolymer in ambient curing temperature. Mater. Manuf. Process. **32**, 461–467 (2017)
184. Matalkah, F., Soroushian, P.: Shelf life of alkali activated cement: effects of storage condition and duration. Constr. Build. Mater. **222**, 664–672 (2019)
185. Bernal, S.A.: Advances in near-neutral salts activation of blast furnace slags. RILEM Tech. Lett. **1**, 39–44 (2016)
186. Alonso, M.M., Gascó, C., Morales, M.M., et al.: Olive biomass ash as an alternative activator in geopolymer formation: a study of strength, durability, radiology and leaching behaviour. Cem. Concr. Compos. **104**, 103384 (2019)
187. Adesanya, E., Ohenoja, K., Di Maria, A., et al.: Alternative alkali-activator from steel-making waste for one-part alkali-activated slag. J. Clean. Prod. **274**, 123020 (2020)
188. Kaya, M., Köksal, F., Nodehi, M., et al.: The effect of sodium and magnesium sulfate on physico-mechanical and microstructural properties of Kaolin and ceramic powder-based geopolymer mortar. Sustainability **14**, 13496 (2022)
189. Sturm, P., Gluth, G.J.G., Brouwers, H.J.H., Kühne, H.C.: Synthesizing one-part geopolymers from rice husk ash. Constr. Build. Mater. **124**, 961–966 (2016)
190. Hajimohammadi, A., Provis, J.L., Van Deventer J.S.J.: One-part geopolymer mixes from geothermal silica and sodium aluminate. In: AIChE Annual Meeting Conference on Proceedings (2008)
191. Gluth, G.J.G., Lehmann, C., Rübner, K., Kühne, H.C.: Geopolymerization of a silica residue from waste treatment of chlorosilane production. Mater. Struct. Constr. **46**, 1291–1298 (2013)
192. Feng, D., Provis, J.L., Van Deventer, J.S.J.: Thermal activation of albite for the synthesis of one-part mix geopolymers. J. Am. Ceram. Soc. **95**, 565–572 (2012)
193. Peng, M.X., Wang, Z.H., Shen, S.H., et al.: Alkali fusion of bentonite to synthesize one-part geopolymeric cements cured at elevated temperature by comparison with two-part ones. Constr. Build. Mater. **130**, 103–112 (2017)
194. Ke, X., Bernal, S.A., Ye, N., et al.: One-part geopolymers based on thermally treated red Mud/NaOH blends. J. Am. Ceram. Soc. **98**, 5–11 (2015)
195. Liu, Q., Li, X., Cui, M., et al.: Preparation of eco-friendly one-part geopolymers from gold mine tailings by alkaline hydrothermal activation. J. Clean. Prod. **298**(126806), 6 (2021)
196. Ahmad, M.R., Qian, L.P., Fang, Y., et al.: A multiscale study on gel composition of hybrid alkali-activated materials partially utilizing air pollution control residue as an activator. Cem. Concr. Compos. **136**, 104856 (2023)
197. Riaz Ahmad, M., Khan, M., Wang, A., et al.: Alkali-activated materials partially activated using flue gas residues: an insight into reaction products. Constr. Build. Mater. **371**, 130760 (2023)
198. Willson-Levy, R., Peled, A., Klein-BenDavid, O., Bar-Nes, G.: Development of One-part geopolymers based on industrial carbonate waste. Constr. Build. Mater. **365**, 130009 (2023)

199. Refaat, M., Mohsen, A., Nasr, E.S.A.R., Kohail, M.: Utilization of optimized microwave sintering to produce safe and sustainable one-part alkali-activated materials. Sci. Rep. **13**, 1–22 (2023)
200. Baláž, P., Achimovicová, M., Baláž, M., et al.: Hallmarks of mechanochemistry: from nanoparticles to technology. Chem. Soc. Rev. **42**, 7571–7637 (2013)
201. Matalkah, F., Xu, L., Wu, W., Soroushian, P.: Mechanochemical synthesis of one-part alkali aluminosilicate hydraulic cement. Mater. Struct. Constr. **50**, 1–12 (2017)
202. Matalkah, F., Alomari, A.H., Soroushian, P.: Scaled-up production of alkali-activated cement in the presence of carbon dioxide for concrete construction. Case Stud. Constr. Mater. **13**, e00463 (2020)
203. Hosseini, S., Brake, N.A., Nikookar, M., et al.: Mechanochemically activated bottom ash-fly ash geopolymer. Cem. Concr. Compos. **118**, 103976 (2021)
204. Matalkah, F., Soroushian, P.: Role of CO2 in enhancing geopolymer properties formulated with fluidized bed combustion ash. J. CO2 Util. **71**, 102462 (2023)
205. Abbas, I.S., Abed, M.H., Canakci, H.: Development and characterization of eco- and user-friendly grout production via mechanochemical activation of slag/rice husk ash geopolymer. J. Build. Eng. **63**, 105336 (2023)
206. Pol Segura, I., Ranjbar, N., Juul Damø, A., et al.: A review: alkali-activated cement and concrete production technologies available in the industry. Heliyon **9**, e15718 (2023)
207. Guo, S., Wu, Y., Jia, Z., et al.: Sodium-based activators in alkali-activated materials: classification and comparison. J. Build. Eng. **70**, 106397 (2023)
208. Filipponi, A., Masi, G., Bignozzi, M.C.: Pressing metakaolin-based one-part geopolymers: influence of the mix design on microstructural and physical properties. Ceram. Int. **48**, 5814–5823 (2022)
209. Abed, M.H., Abbas, I.S., Canakci, H.: Effect of glass powder on the rheological and mechanical properties of slag-based mechanochemical activation geopolymer grout. Eur. J. Environ. Civ. Eng. **27**, 3628–3652 (2023)
210. Hamid Abed, M., Sabbar Abbas, I., Hamed, M., Canakci, H.: Rheological, fresh, and mechanical properties of mechanochemically activated geopolymer grout: a comparative study with conventionally activated geopolymer grout. Constr. Build. Mater. **322**, 126338 (2022)
211. Choo, H., Lim, S., Lee, W., Lee, C.: Compressive strength of one-part alkali activated fly ash using red mud as alkali supplier. Constr. Build. Mater. **125**, 21–28 (2016)
212. Perumal, P., Nguyen, H., Carvelli, V., et al.: High strength fiber reinforced one-part alkali activated slag composites from industrial side streams. Constr. Build. Mater. **319**, 126124 (2022)
213. Elzeadani, M., Bompa, D.V., Elghazouli, A.Y.: Experimental assessment and constitutive modelling of rubberised one-part alkali-activated concrete. Constr. Build. Mater. **353**, 129161 (2022)
214. D'alessandro, A., Coffetti, D., Crotti, E., et al.: Self-sensing properties of green alkali-activated binders with carbon-based nanoinclusions. Sustainability **12**, 1–13 (2020)
215. Adesanya, E., Ohenoja, K., Luukkonen, T., et al.: One-part geopolymer cement from slag and pretreated paper sludge. J. Clean. Prod. **185**, 168–175 (2018)
216. Migunthanna, J., Rajeev, P., Sanjayan, J.: Waste clay brick as a part binder for pavement grade geopolymer concrete. Int. J. Pavement Res. Technol. **17**, 1450–1467 (2024)
217. Rasmus, J., Ohenoja, K., Kinnunen, P., Illikainen, M.: Effect of green liquor dregs as an alkali source for alkali-activated blast furnace slag mortar. Case Stud. Constr. Mater. **18**, e01950 (2023)
218. Ren, J., Sun, H., Li, Q., et al.: Experimental comparisons between one-part and normal (two-part) alkali-activated slag binders. Constr. Build. Mater. **309**, 125177 (2021)
219. Zhang, H.Y., Liu, J.C., Wu, B.: Mechanical properties and reaction mechanism of one-part geopolymer mortars. Constr. Build. Mater. **273**, 121973 (2021)

220. Samarakoon, M.H., Ranjith, P.G., Duan, W.H., De Silva, V.R.S.: Properties of one-part fly ash/slag-based binders activated by thermally-treated waste glass/NaOH blends: a comparative study. Cem. Concr. Compos. **112**, 103679 (2020)
221. van Deventer, J.S.J.: Valorisation of slag in construction: so much more than just technology. In: 5th Slag Valorisation Symposium, pp. 301–311 (2017)